Integrin α5β1 facilitates cancer cell invasion through enhanced contractile forces

Claudia Tanja Mierke[1,*], Benjamin Frey[2], Martina Fellner[3], Martin Herrmann[4] and Ben Fabry[3]

[1]Faculty of Physics and Earth Science, Institute for Experimental Physics I, Soft Matter Physics Division, University of Leipzig, 04103 Leipzig, Germany
[2]Department of Radiation Oncology, Radiation Immunobiology Group, University Hospital Erlangen, 91054 Erlangen, Germany
[3]Center for Medical Physics and Technology, Biophysics Group, Friedrich-Alexander-University of Erlangen-Nuremberg, 91052 Erlangen, Germany
[4]Department of Internal Medicine III, Institute of Clinical Immunology and Rheumatology, University Hospital Erlangen, 91054 Erlangen, Germany
*Author for correspondence (claudia.mierke@t-online.de)

Accepted 28 September 2010
Journal of Cell Science 124, 369-383

doi:10.1242/jcs.071985

Summary

Cell migration through connective tissue, or cell invasion, is a fundamental biomechanical process during metastasis formation. Cell invasion usually requires cell adhesion to the extracellular matrix through integrins. In some tumors, increased integrin expression is associated with increased malignancy and metastasis formation. Here, we have studied the invasion of cancer cells with different α5β1 integrin expression levels into loose and dense 3D collagen fiber matrices. Using a cell sorter, we isolated from parental MDA-MB-231 breast cancer cells two subcell lines expressing either high or low amounts of α5β1 integrins (α5β1^{high} or α5β1^{low} cells, respectively). α5β1^{high} cells showed threefold increased cell invasiveness compared to α5β1^{low} cells. Similar results were obtained for 786-O kidney and T24 bladder carcinoma cells, and cells in which the α5 integrin subunit was knocked down using specific siRNA. Knockdown of the collagen receptor integrin subunit α2 also reduced invasiveness, but to a lesser degree than knockdown of integrin subunit α5. Fourier transform traction microscopy revealed that the α5β1^{high} cells generated sevenfold greater contractile forces than α5β1^{low} cells. Cell invasiveness was reduced after addition of the myosin light chain kinase inhibitor ML-7 in α5β1^{high} cells, but not in α5β1^{low} cells, suggesting that α5β1 integrins enhance cell invasion through enhanced transmission and generation of contractile forces.

Key words: Acto-myosin cytoskeleton, Cell stiffness, Steric hindrance

Introduction

Deregulated cell–cell and cell–matrix interactions and enhanced cell invasion promote the malignancy of neoplasms and determine their ability to form metastases in distant regions (Batlle et al., 2000; Behrens et al., 1989; Cano et al., 2000; Danen et al., 2005; De Craene et al., 2005; Frixen et al., 1991; Vleminckx et al., 1991). The process of metastasis formation involves multiple steps that include the segregation of tumor cells from a primary tumor, their migration through connective tissue rich in collagen type I, intravasation into blood or lymph vessels, adhesion to the endothelium and, possibly but not necessarily, subsequent extravasation and further tissue invasion (Al-Mehdi et al., 2000; Steeg, 2006). The adhesion, transmigration and invasion steps involve integrin cell surface molecules (Buckley et al., 1996; Leroy-Dudal et al., 2005; Voura et al., 2001).

Integrins, a family of transmembrane adhesion receptors composed of non-covalently linked α- and β-subunits, mediate transmembrane connections between the actin cytoskeleton and the extracellular matrix (ECM) (Damsky et al., 1985; Hemler et al., 1987; Neff et al., 1982). In adherent cells, these connections are organized in discrete clusters as focal adhesions (Geiger et al., 2001). Focal adhesions anchor cells to their substrate and transmit traction forces generated by the contractile (acto-myosin) cytoskeleton (Balaban et al., 2001; Loftus and Liddington, 1997; Palecek et al., 1997; Zaman et al., 2006). The contractile pre-stress carried by the actin cytoskeleton in turn is essential for controlling cell shape and for providing mechanical integrity (Elson, 1988; Giannone and Sheetz, 2006). Contractile pre-stress and focal adhesions are linked not only mechanically but also through signaling processes (Friedland et al., 2009; Gallant et al., 2005; Geiger et al., 2001; Paszek et al., 2005). For instance, contractile forces influence the size of focal adhesions (Balaban et al., 2001), and focal adhesion proteins such as vinculin control the magnitude of the pre-stress (Mierke et al., 2008a).

Adhesion molecules have been identified either to enhance tumor metastasis, e.g. αvβ3 (Voura et al., 2001) and α6β4 (Mukhopadhyay et al., 1999; Owens et al., 2003), or to reduce tumor metastasis, e.g. E-cadherin (Frixen et al., 1991). The roles of other adhesion molecules such as the integrin α3 subunit depend on the type of cancer and can be associated with increased or decreased malignancy (Kreidberg, 2000). Reports on the role of the integrin α5β1 are controversial and show both positive correlations (Caswell et al., 2008; Caswell et al., 2007; Qian et al., 2005; Sawada et al., 2008; Wu et al., 2006) or negative correlations with metastasis formation or tumor malignancy (Schirner et al., 1998; Tani et al., 2003; Taverna et al., 1998).

The aim of this study was to analyze the role of the α5β1 integrin for cancer cell invasion under controlled in-vitro conditions, and to characterize the biomechanical invasion strategy that is activated by α5β1 integrins. We used 2.4 mg/ml synthetic three-dimensional (3D) collagen matrices with subcellular-sized pores as an ECM substrate (Mickel et al., 2008; Mierke et al., 2008c). The invasiveness and the speed of migration in such a system depend primarily on biomechanical processes including cell adhesion and

de-adhesion (Friedl and Brocker, 2000), cytoskeletal remodeling (Mierke et al., 2008c) and protrusive force generation (Friedl and Brocker, 2000; Webb et al., 2004), and on matrix properties such as stiffness, pore size, protein composition, and enzymatic degradation (Zaman et al., 2006). As previously reported, cell invasion strategies (mesenchymal or amoeboid migration) and invasion speed depend on the balance of these parameters (Wolf et al., 2003).

In this study, we investigated the invasion of 51 tumor lines in 3D collagen matrices and observed that cell invasiveness significantly correlated with α5 integrin expression. Subclones of cancer lines selected for high α5 integrin expression displayed an increased invasiveness in 3D collagen matrices, whereas knockdown of the α5 integrin subunit decreased cancer cell invasion. We systematically tested the integrin-type specificity of the invasion-enhancing effect and measured cell adhesion strength, cytoskeletal remodeling and traction force generation. In addition, we controlled the steric hindrance and adhesiveness of the ECM by varying protein composition and collagen density, and we blocked enzymatic matrix degradation. We found that the α5β1 integrin contributes substantially to the invasive capability of cancer cells by promoting the transmission and generation of contractile forces.

Results

Invasive cancer cells display increased α5β1 integrin expression

We analyzed whether cell surface expression of integrins is correlated with the invasive behavior of common cancer cell lines. Cell invasiveness of 51 cancer cell lines was determined using a 3D collagen matrix invasion assay in which cancer cells were seeded on top of a 500-μm thick collagen type I fiber network (Fig. 1A–D). Cells adhered to (Fig. 1B,C) and invaded spontaneously into (Fig. 1D–I) these collagen gels. Invasive cells were elongated (Fig. 1H) and showed multiple filopodia (Fig. 1E–G) with a dense cytoskeletal network (Fig. 1I). The invasiveness of each cell line was quantified by an invasion score that is defined as number density of invasive cells multiplied by the average invasion depth (Mierke et al., 2008c). Cancer cell lines with an invasion score below 0.1 mm^{-1} were defined as non-invasive, and above 0.1 mm^{-1} as invasive. A total of 24 cell lines were found to be invasive, and 27 cell lines to be non-invasive (supplementary material Table S1).

The expression of two integrins (αvβ3, αvβ5) and four integrin subunits (β1, α3, α4, α5) on each cell line was analyzed by flow cytometry (Fig. 2 and supplementary material Table S1). The expression of integrin subunits α3 and α5 as well as αvβ3 integrin

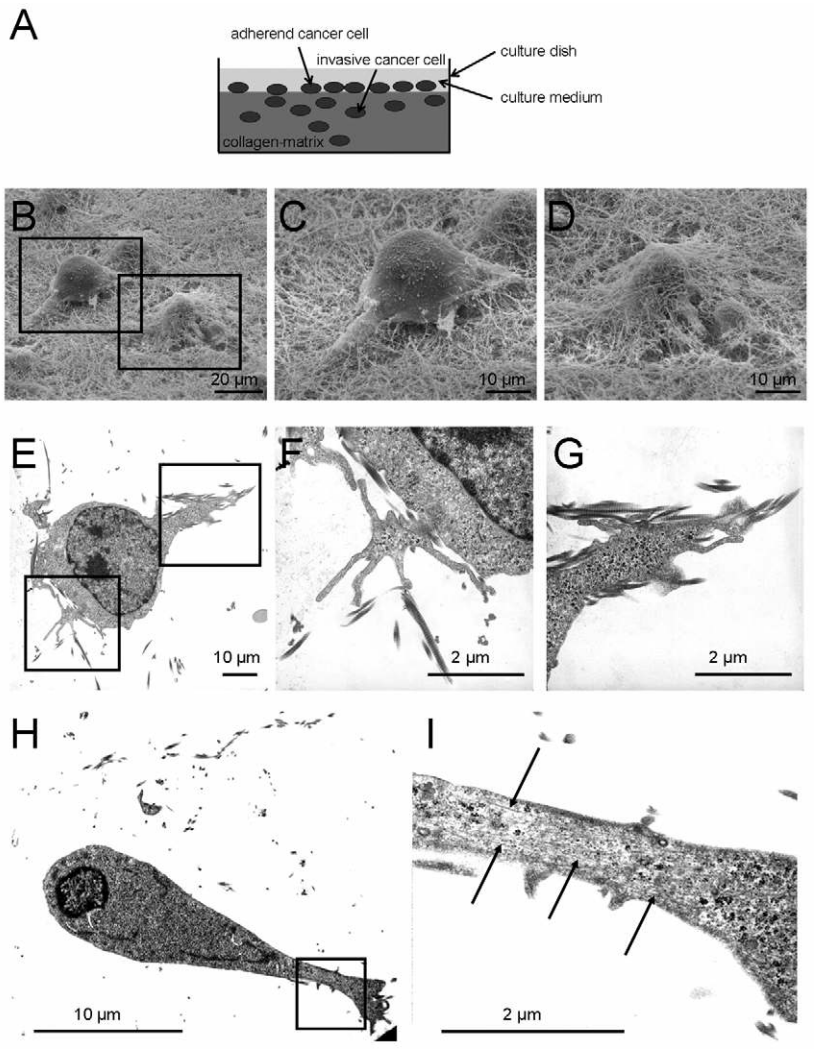

Fig. 1. Invasion assay. (**A**) Schematic of the cancer cell invasion assay. (**B–D**) SEM images of MDA-MB-231 breast cancer cells show that the cells adhered on (C) or invaded in 3D collagen matrices (D). (**E–G**) TEM images show that invasive MDA-MB-231 cells formed filopodia inside 3D collagen matrices. (E) Overview image. (F,G) Magnifications of boxed areas in E. (**H**,**I**) Cancer cells that invaded into 3D collagen matrices show a dense cytoskeletal network. (I) Magnification of boxed area in H. Arrows point to the dense cytoskeletal network inside an invasive MDA-MB-231 cell.

was significantly upregulated on invasive cancer lines (Fig. 2), indicating that these integrins could be functionally involved in cancer cell invasion.

High α5β1 integrin expression leads to enhanced cell invasion

To investigate the effect of the α5β1 expression on invasion, we isolated from the parental breast cancer line MDA-MB-231 two subcell lines that expressed either high or low amounts of α5β1 integrins on their cell surface (Fig. 3A). In the following, these subcell lines are referred to as α5β1^{low} and α5β1^{high} cells. Between these subcell lines, the difference in the expression of α5 integrin was 28.4-fold (Fig. 3B), and the difference in the expression of β1 integrin was 2.8-fold (Fig. 3D). Using cytofluorometry, we confirmed that the α5β1 integrin expression levels were stable during culture for more than 100 passages (supplementary material Fig. S1). All experiments in this study were performed on cells derived from a single isolation that had been obtained by cell sorting with respect to α5 integrin subunit expression. In independent experiments, we repeated the sorting of parental cells in total five times over the course of 3 years, and each time we were able to establish a stable α5β1^{low} and α5β1^{high} phenotype with similarly high differences in the invasion behavior (data not shown). This finding confirms that the α5β1^{low} and α5β1^{high} phenotypes can be obtained reproducibly.

The percentage of cells that were able to invade into a 3D collagen matrix was 15-fold higher for α5β1^{high} than for α5β1^{low} cells (Fig. 3C). In addition, the invasion profile (cumulative probability) of the invasive cells showed that α5β1^{high} cells invaded deeper into the ECM (Fig. 3E). The aspect ratio of the invaded α5β1^{high} cells was fourfold higher than that of α5β1^{low} cells (Fig. 3F). To investigate whether the effect of the α5β1 expression on invasiveness is cancer cell-type specific, we isolated α5β1^{high}, α5β1^{medium} and α5β1^{low} cells from 786-O human kidney carcinoma cells (9.4-fold difference between α5β1^{high} and α5β1^{low}) as well as α5β1^{high} and α5β1^{low} cells from T24 bladder carcinoma cells (sixfold difference) (supplementary material Fig. S2). We found that the cell invasiveness of α5β1^{high} cells derived from 786-O and T24 cells was higher than that of α5β1^{medium} or α5β1^{low} cells, confirming that the cell invasiveness increases with integrin α5β1 expression levels in several cancer cell-types.

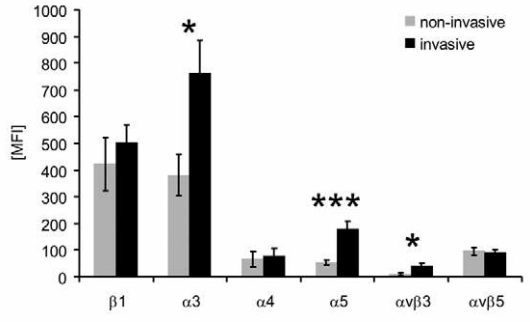

Fig. 2. Integrin expression of invasive and non-invasive cancer cells correlate with invasion. Expression of various integrins was measured in invasive (n=24), and non-invasive cancer cell lines (n=27). Invasive cells expressed twofold higher levels of integrin α3, threefold higher levels of α5 and fourfold higher levels of αvβ3. Data are presented as mean ± s.e.m. *P<0.05, ***P<0.001. MFI, mean fluorescence intensities.

Speed and persistence of 3D cell migration is enhanced in α5β1^{high} cells

To characterize the 3D migration behavior of MDA-MB-231 α5β1^{high} and α5β1^{low} cells, we determined the speed and persistence of migration from the mean squared displacement (MSD) of individual cells using time-lapse video analysis (Fig. 3G–I). The MSD was computed from the cell trajectories recorded during 2 hours of cell migration (Fig. 3G). The MSD increased with time according to a power-law relationship (Dieterich et al., 2008), $MSD=D(t/t_0)^{\beta}$, where t_0 is the time interval between two measurements (1 minute), the apparent diffusivity D is a measure of the migration speed (Fig. 3H), and the exponent β is a measure of the persistence (Fig. 3I) (Raupach et al., 2007). The apparent diffusivity D was increased eightfold in α5β1^{high} cells (Fig. 3H), corresponding to a 2.8-fold higher migration speed compared with α5β1^{low} cells (Fig. 3G, inset). Moreover, α5β1^{high} cells migrated more persistently, as reflected by their higher β-value (Fig. 3I). These results suggest that increased invasion speed and persistence contributed significantly to the increased α5β1-integrin-mediated cell invasiveness.

Surface expression of other integrins on α5β1^{high} and α5β1^{low} cells

To investigate whether the increased invasiveness seen in α5β1^{high} cells resulted from increased expression of collagen-binding integrins or other ECM-binding integrins, we measured their cell surface expression on α5β1^{high} and α5β1^{low} cells. The expression of collagen-binding integrin subunits α1 and α2 on α5β1^{high} cells was upregulated (2.1-fold and 3.5-fold, respectively) (Fig. 4A), whereas the expression of the laminin-binding integrin subunit α6 was not altered (Fig. 4A), and the expression of the integrin subunit β4 was 1.7-fold decreased on α5β1^{high} cells (supplementary material Fig. S3). Expression of the integrin subunit α4 (data not shown) and of the vitronectin-binding integrin αvβ3 (supplementary material Fig. S3) were low on both subcell lines. These data suggest that the collagen-binding integrin subunits α1 and α2 might play a role in the increased invasiveness of α5β1^{high} cells. Therefore, the impact of the two integrin subunits on cell invasion was investigated.

Inhibition of α5β1-integrin-facilitated cell invasion

To test which integrin was primarily responsible for the increased invasiveness of α5β1^{high} cells, we measured cell invasion under the influence of integrin-blocking antibodies. The addition of 100 μM anti-α5 blocking antibody or 100 μM anti-β1 blocking antibody reduced the percentage of invasive cells to 10% of cells treated with isotype-matched (IgG_1) control antibody. The addition of 100 μM anti-α1 and anti-α2 blocking antibodies reduced the percentage of invasive cells only to 88% and 65%, respectively (Fig. 4D). The invasion depth was greatly reduced after addition of anti-α5 or anti-β1 blocking antibody and was reduced to a lesser degree by the anti-α2 and anti-α1 antibodies (Fig. 4E). These findings demonstrate that α5β1 integrins were mainly responsible for the increased invasiveness of α5β1^{high} cells.

This result was further confirmed using specific siRNA to knockdown the α1, α2 and α5 integrin subunit expression in α5β1^{high} cells. The percentage of siRNA-mediated knockdown was determined by flow cytometry after 3 days (Fig. 4B). A 79.3% knockdown of α5 integrin decreased the percentage of invasive cells in 3D collagen matrices compared to treatment with control siRNA, whereas knockdown of subunits α1 (86.8%) or α2 (66.4%)

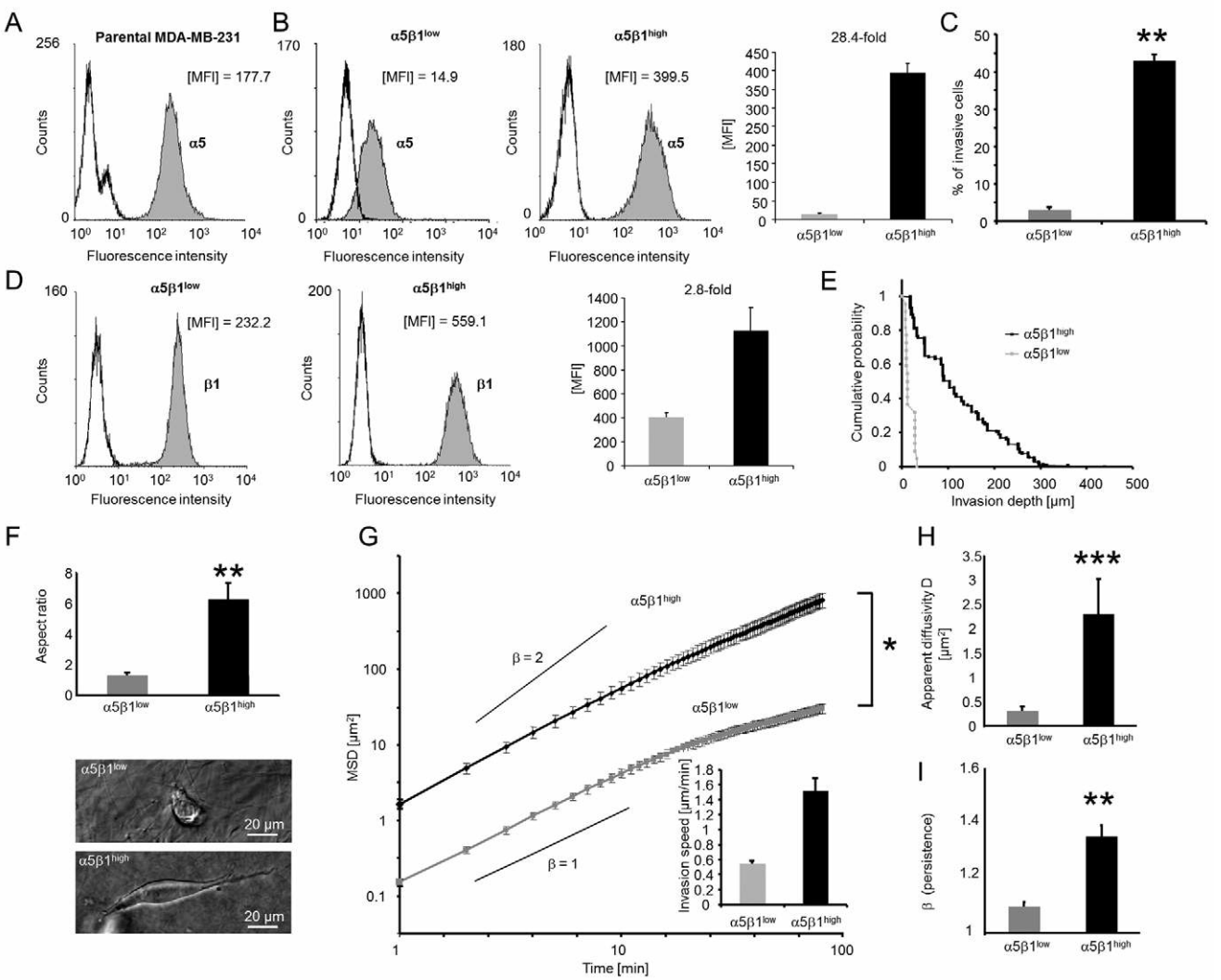

Fig. 3. Effect of α5β1 integrin expression on cell invasion in 3D ECMs. (**A**) α5 integrin subunit expression of parental MDA-MB-231 cells. (**B**) α5 and (**D**) β1 integrin subunit expression of $\alpha5\beta1^{low}$ and $\alpha5\beta1^{high}$ cells. In each histogram, left curves are isotype controls and filled gray curves show integrin expression. One representative experiment out of five is shown. The corresponding bar graphs show MFI values (mean + s.e.m., *n*=5). (**C**) A higher percentage of $\alpha5\beta1^{high}$ cells invaded into 3D ECMs compared to $\alpha5\beta1^{low}$ cells after 3 days. (**E**) Invasion profiles show that $\alpha5\beta1^{high}$ cells migrated deeper into 3D collagen matrices than did $\alpha5\beta1^{low}$ cells. (**F**) Aspect ratio of invaded $\alpha5\beta1^{high}$ and $\alpha5\beta1^{low}$ cells after 3 days. Bright field images of $\alpha5\beta1^{high}$ (lower image, depth 180 μm) and $\alpha5\beta1^{low}$ cells (upper image, depth 68 μm) inside collagen gels. (**G**) The MSD of $\alpha5\beta1^{high}$ cells was significantly greater than that of $\alpha5\beta1^{low}$ cells. Inset: invasion speed of $\alpha5\beta1^{high}$ and $\alpha5\beta1^{low}$ cells in 3D ECMs. Calculated slopes for the power-law exponent β=1 and β=2 are shown. (**H**) The apparent diffusivity was increased in $\alpha5\beta1^{high}$ cells, indicating a higher migration speed. (**I**) The 3D motility of $\alpha5\beta1^{high}$ cells was more persistent than that of $\alpha5\beta1^{low}$ cells, as shown by a higher β. **P*<0.05, ***P*<0.01, ****P*<0.001.

had a minor effect (Fig. 4F). α5 integrin knockdown also decreased the invasion depth, whereas the effect of α1 or α2 knockdown was smaller (Fig. 4G). We confirmed that knockdown of the α1 or α2 subunits caused no changes in the cell surface expressions of the other α-integrin subunits (supplementary material Fig. S4). Similar results were obtained using four other α5-specific siRNAs (knockdown of 66.0–79.4%, data not shown). We confirmed that the cell surface expressions of the collagen-binding α1 and α2 integrin subunits were not altered by knockdown of the α5 subunit (supplementary material Fig. S5).

To account for the functional role of α2β1 integrins, we performed experiments with MDA-MB-231 subclones that were sorted for $\alpha2\beta1^{low}$ and $\alpha2\beta1^{high}$ expression. The α2 integrin expression on $\alpha2\beta1^{high}$ cells was 14-fold higher than on $\alpha2\beta1^{low}$ cells (Fig. 4C). The expression levels of α5 integrins were similarly high in both the $\alpha2\beta1^{low}$ and $\alpha2\beta1^{high}$ cell lines. The invasiveness of $\alpha2\beta1^{high}$ cells increased compared to $\alpha2\beta1^{low}$ cells (Fig. 4H,I), thus confirming our siRNA knockdown results. However, the $\alpha2\beta1^{low}$ cells were still able to invade into 3D ECMs, which suggests a less pronounced dependence of cell invasion on α2 integrins than on α5 integrins.

Role of matrix degradation for α5β1-integrin-mediated cell invasiveness

Cell invasion has been reported to be associated with increased secretion of the membrane-type 1 matrix metalloproteinase (MT1-MMP), a major collagen-degrading proteinase (Wolf et al., 2003). Here, we analyzed whether differences in MT1-MMP cell surface

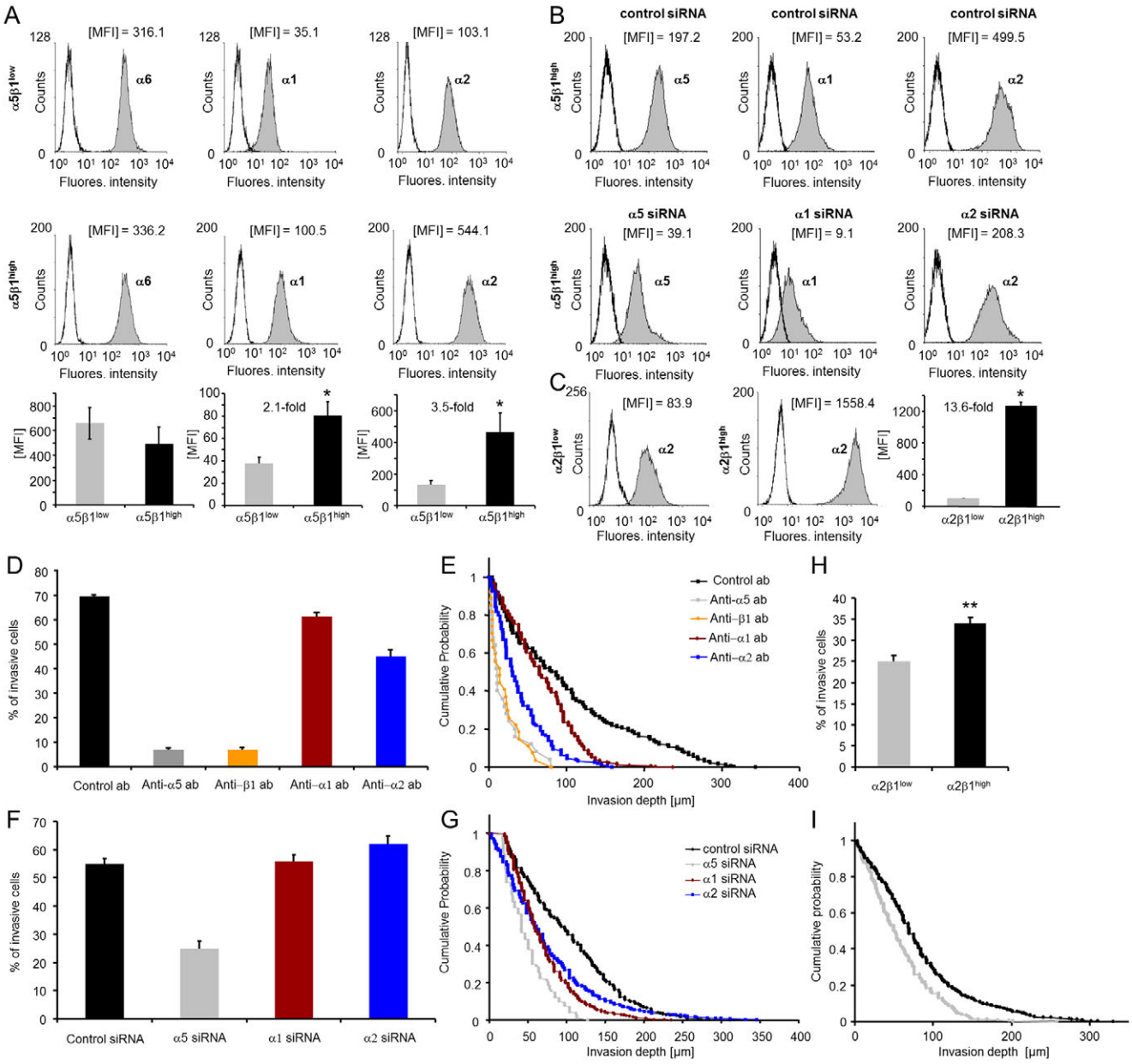

Fig. 4. Integrin expression of subcell lines and inhibition of α5β1-integrin-mediated cell invasion. (**A**) Analysis by flow cytometry of both subclones revealed different α1, α2 and α6 integrin expression. One representative experiment out of six is shown. The corresponding bar graphs show MFI values (mean + s.e.m., *n*=6). (**B**) Flow cytometry analysis of integrin expression on $\alpha5\beta1^{high}$ cells after addition of unspecific control siRNA (top row) or specific siRNAs (bottom row) targeting integrins α5 (left), α1(middle) and α2 (right). One representative experiment out of at least three is shown. (**C**) Analysis by flow cytometry of $\alpha2\beta1^{low}$ and $\alpha2\beta1^{high}$ subclones. One representative experiment out of at least five is shown. The bar graphs show MFI values (mean + s.e.m., *n*=5). (**D**) Percentage of invasive cells and (**E**) invasion profiles of $\alpha5\beta1^{high}$ cells after addition of 100 μM of control antibodies (black) or blocking antibodies against integrins α5 (gray), β1 (orange), α1 (red) and α2 (blue). (**F**) Percentage of invasive cells and (**G**) invasion profiles of $\alpha5\beta1^{high}$ cells transfected with control siRNA (black) or with siRNAs targeting integrins α5 (gray), α1 (red) and α2 (blue). (**H**) Percentage of invasive cells and (**I**) invasion profiles of $\alpha2\beta1^{low}$ and $\alpha2\beta1^{high}$ subclones. **P*<0.05, ***P*<0.01.

expression were responsible for differences in cell invasiveness between $\alpha5\beta1^{high}$ and $\alpha5\beta1^{low}$ cells. The expression of MT1-MMP was upregulated in selected invasive cancer lines compared to non-invasive cancer cell lines (supplementary material Fig. S6); however, the expression of MT1-MMP did not differ between $\alpha5\beta1^{high}$ and $\alpha5\beta1^{low}$ cells (supplementary material Fig. S6). Because fibronectin is the main ligand for α5β1 integrins, we also considered the expression of the fibronectin-degrading enzyme matrilysin (MMP-7). The expression of MMP-7 was increased twofold on $\alpha5\beta1^{high}$ cells compared with $\alpha5\beta1^{low}$ cells (supplementary material Fig. S6).

The overall activity of proteolytic enzymes was investigated by adding a protease inhibitor cocktail (PI) to $\alpha5\beta1^{high}$ and $\alpha5\beta1^{low}$ cells prior to the start of the invasion assay. We found that the percentage of invasive $\alpha5\beta1^{high}$ cells after PI treatment was decreased, and that these cells did not migrate beyond 210 μm into

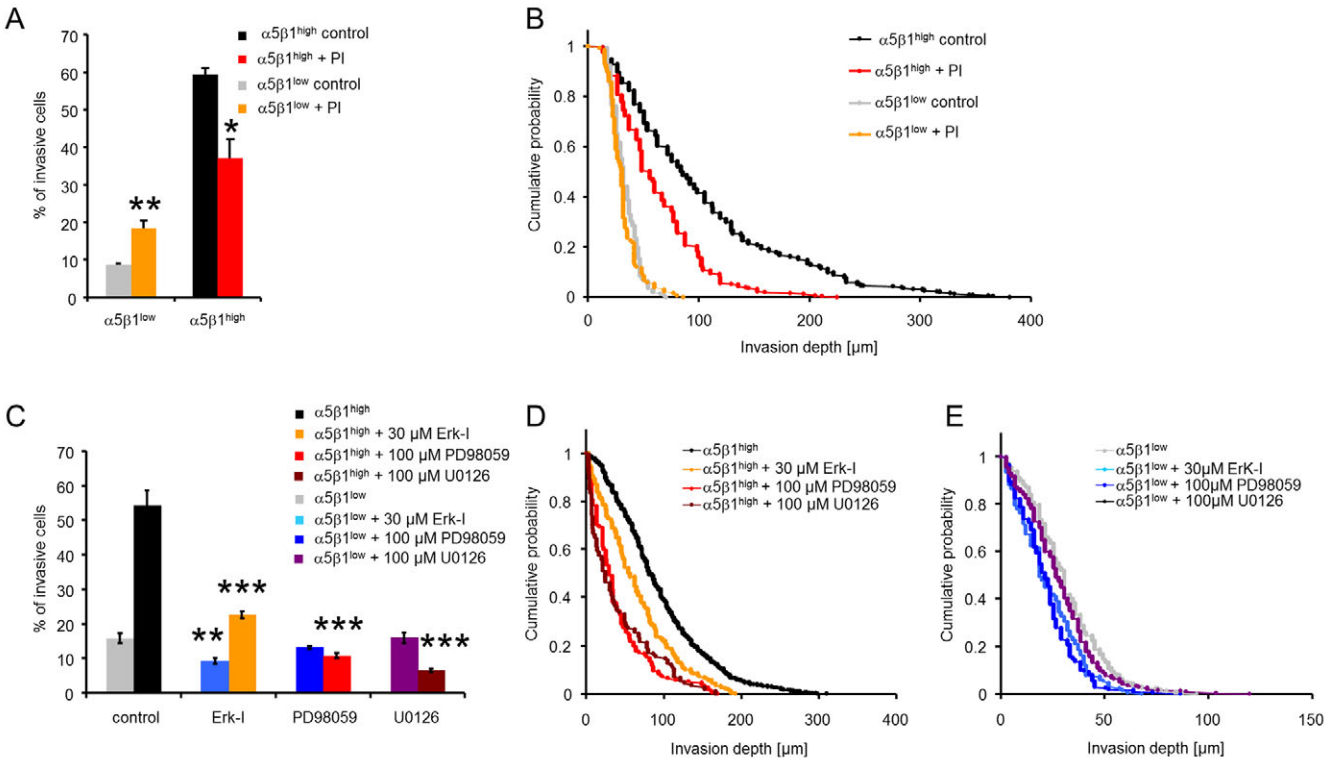

Fig. 5. Effect of enzymatic ECM degradation and ERK1/2 inhibition on cell invasion. (**A**) Percentage of invasive α5β1^{high} cells (red) was reduced after addition of a protease inhibitor cocktail (PI), whereas the number of invasive cells was increased in α5β1^{low} cells (orange). (**B**) The invasion profile shows that the PI-treated α5β1^{high} cells did not invade as deep as control cells (DMSO-treated), whereas the invasion profile was not altered in PI-treated α5β1^{low} cells. (**C–E**) The percentage of invasive α5β1^{high} cells (C) and their invasion depths (D) were decreased after addition of the inhibitors 328005 (30 μM; Erk-1), PD98059 (100 μM) or U0126 (100 μM), whereas the percentage of invasive α5β1^{low} cells (C) was slightly reduced and their invasion depths (E) were only marginally altered. *P<0.05, **P<0.01, ***P<0.001.

the 3D collagen matrices (Fig. 5A). The percentage of invasive α5β1^{low} cells was increased after PI treatment (Fig. 5A), but their invasion profile was only marginally affected (Fig. 5B). Nonetheless, the differences in cell invasiveness between α5β1^{high} and α5β1^{low} cells after protease inhibition remained large. Taken together, these data show that the enzymatic digestion of the 3D collagen matrices is not a prerequisite for invasion of these cells, and that differences in the protease activity can only account for α5β1-integrin-facilitated cell invasion to a slight degree.

Role of growth factor signaling in α5β1-integrin-mediated cell invasiveness

Growth factor receptors and associated signaling pathways have been previously shown to contribute to adhesion-dependent growth and cell migration (Festuccia et al., 2005; Gilcrease et al., 2009; Lund-Johansen et al., 1990). To test the hypothesis that growth factor signaling was involved in α5β1-integrin-mediated cell invasiveness, we inhibited extracellular signal-regulated kinase 1 and 2 (ERK1/2), which are central proteins in EGF-receptor-mediated signaling. We added 30 μM of the ERK1/2 inhibitor 328005, 100 μM of the MAP-kinase kinase (MEK) inhibitor PD98059 or 100 μM of the MEK inhibitor U0126 to the cells during 3 days of cell invasion in a 3D collagen matrix. The ERK inhibitor 328005 slightly reduced the percentage of invasive cells and the invasion depths (Fig. 5C–E). The MEK inhibitors PD98059 and the U0126 reduced the invasiveness of α5β1^{high} as indicated by the decreased number of invasive cells and the lower invasion depth (Fig. 5C–E). Taken together, these data leave open the possibility that α5β1-integrin-facilitated cell invasion is mediated by growth factor receptors and ERK1/2 signaling.

Effect of α5β1 integrins on cell morphology, focal adhesions and spreading area

α5β1^{high} and α5β1^{low} cells were cultured for 24 hours on glass coverslips coated with collagen type I, fibronectin, RGD peptide and vitronectin. The cell spreading area of α5β1^{high} cells on collagen was increased twofold compared with α5β1^{low} cells (Fig. 6A,B; P<0.0001). α5β1^{high} cells showed well-defined stress fibers and prominent focal adhesions (Fig. 6C, right images), whereas α5β1^{low} cells exhibited mostly cortical actin, no cell-spanning stress fibers and weakly stained focal adhesions (Fig. 6C, left images). However, the overall β-actin content did not differ between α5β1^{high} cells and α5β1^{low} cells (supplementary material Fig. S7).

The α5β1^{high} cells displayed a fibroblast-like, elongated phenotype, whereas the α5β1^{low} cells were more rounded and epithelial-like (Fig. 6C). The number of focal adhesions per cell was significantly increased in α5β1^{high} cells, independent of the ECM protein on which the cells were cultured (Fig. 6D). In addition, the expression level of the focal adhesion protein vinculin was higher in α5β1^{high} cells than in α5β1^{low} cells (supplementary material Fig. S7). These findings suggest that the pronounced F-actin cytoskeleton and the associated focal adhesion sites of α5β1^{high} cells might facilitate the generation and transmission of increased contractile forces, which we subsequently tested.

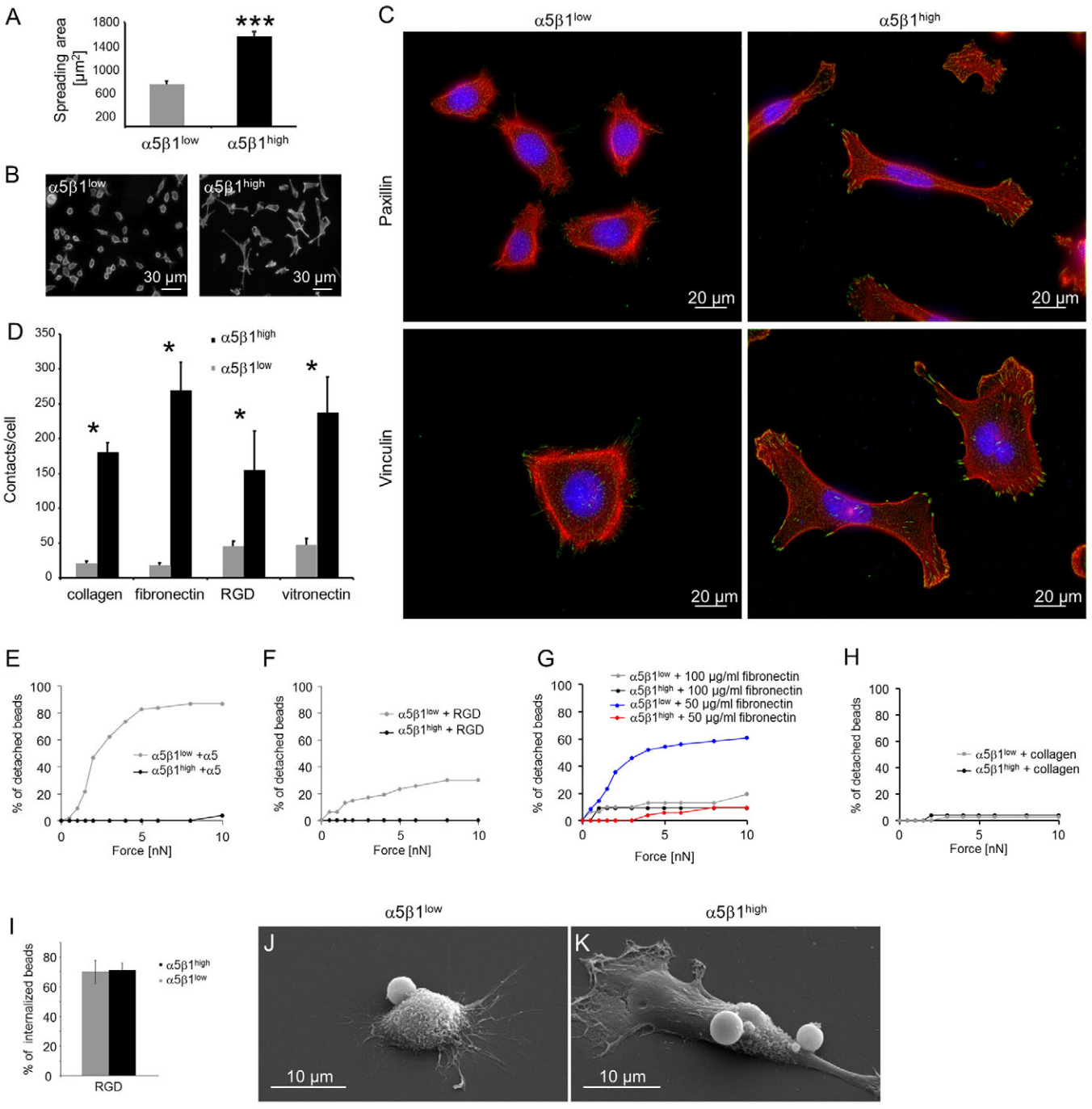

Fig. 6. Adhesion of α5β1^{high} and α5β1^{low} cells. (**A**) Spreading area of α5β1^{high} and α5β1^{low} cells after 24 hours of adhesion to collagen-coated glass substrates. (**B**) Representative fluorescence images of α5β1^{high} (right) and α5β1^{low} (left) cells stained for actin with Alexa-Fluor-546-conjugated phalloidin. These images were used to determine the spreading area. (**C**) Fluorescence images of α5β1^{high} (right) and α5β1^{low} (left) cells stained for actin with Alexa-Fluor-546-conjugated phalloidin (red) and Hoechst 33342 for DNA (blue). Focal adhesions were stained with antibodies against vinculin (bottom) or paxillin (top) (green). (**D**) The number of adhesion contacts per cell (vinculin stained) was significantly increased in α5β1^{high} as compared with α5β1^{low} cells after 24 hours of adhesion on ECM proteins. (**E**,**F**) Increased bond stability (bead detachment) of integrin α5β1^{high} cells towards anti-α5-antibody-coated (10 μg/ml antibody) beads (E) and 100 μg/ml RGD-peptide-coated beads (F) compared to α5β1^{low} cells. (**G**,**H**) Bond stability of both subcell lines towards beads coated with100 μg/ml or 50 μg/ml fibronectin (G) and 100 μg/ml collagen (H). (**I**) Percentages of internalized RGD-peptide-coated beads after 30 minutes of incubation with α5β1^{high} and α5β1^{low} cells. (**J**,**K**) Representative SEM images of α5β1^{low} (J) and α5β1^{high} (K) cells that bound or internalized RGD peptide beads. *P<0.05, ***P<0.001.

Adhesion strength towards collagen or fibronectin

To test whether differences in the invasiveness between α5β1^{high} and α5β1^{low} cells are associated with differences in their matrix adhesion strength, we applied step-wise increasing forces to integrin-receptor-bound beads using magnetic tweezers. We then recorded the minimum force at which the beads detached from the

cells. Detachment forces for beads coated with α5 integrin antibody and RGD peptide were decreased in α5β1^{low} cells compared with α5β1^{high} cells (Fig. 6E,F), whereas 100 μg/ml fibronectin-coated beads (Fig. 6G) and collagen-coated beads (Fig. 6H) showed no differences between the subcell lines at forces up to 10 nN. A reduced adhesion strength of the α5β1^{low} cells towards fibronectin, however, emerged after a reduction of the fibronectin density on the beads by lowering the coating concentration from 100 μg/ml to 50 μg/ml (Fig. 6G). Scanning electron microscopy (SEM) revealed that α5β1^{high} and α5β1^{low} cells were both able to bind and internalize beads coated with RGD peptide (Fig. 6I–K), indicating that α5β1 integrin is functional on both subcell lines.

Cell stiffness is increased in α5β1^{high} cells

Differences in stress fiber formation between α5β1^{high} and α5β1^{low} cells suggest that these two cell lines might differ in cell stiffness. Cell stiffness was measured using magnetic tweezer microrheology (Fig. 7A). Forces of up to 10 nN were applied to super-paramagnetic beads coated with fibronectin. The bead displacement during a step-wise increase in force (creep measurement) followed a power law as described elsewhere (Mierke et al., 2008a). α5β1^{high} cells were significantly stiffer than α5β1^{low} cells (Fig. 7B; $P<0.001$). Cell stiffness increased with increasing forces by similar amounts (5.4-fold in α5β1^{low} cells and fourfold in α5β1^{high} cells, Fig. 7A). As shown later, these differences in cell stiffness are mostly attributable to differences in the acto-myosin contractility (Wang et al., 2001).

Cytoskeletal remodeling dynamics is increased in α5β1^{high} cells

Cytoskeletal remodeling dynamics was measured using two methods. First, we compared the power-law exponent *b* of the creep modulus measured with magnetic tweezer microrheology. The power-law exponent *b* characterizes the visco-elastic response of cells and can assume values between 0 for an elastic solid and 1 for a viscous fluid. Exponent *b* was increased in α5β1^{high} cells at external forces of up to 4 nN, indicating that these cells were more fluid-like (Fig. 7B). Second, we analyzed the spontaneous motion of fibronectin-coated beads over 5 minutes and measured their MSD (Fig. 7C). The MSD was also fitted to a power law as described above for whole-cell movements. The apparent diffusivity *D* (Fig. 7D) was significantly increased in α5β1^{high} cells, indicating that the cytoskeletal remodeling dynamics was increased in these cells. The power-law exponent β for the MSD was also increased in α5β1^{high} cells and showed that the motion of beads bound to the acto-myosin cytoskeleton is more directed compared with α5β1^{low} cells (Fig. 7E). These data are consistent with the whole-cell migration data presented above (Fig. 3G–I) and suggest that the increased migration speed of α5β1^{high} cells in 3D collagen matrices was facilitated by increased cytoskeletal remodeling dynamics.

Contractile force generation is increased in α5β1^{high} cells

To analyze whether differences in the invasiveness of both subcell lines could be explained by their altered ability to generate contractile forces, tractions of α5β1^{high} and α5β1^{low} cells on RGD-peptide-coated polyacrylamide gels (*E*=5.4 kPa) were determined. Fluorescence-activated cell sorting (FACS) analysis showed that the expression of αvβ3 integrins on the two subcell lines was below the detection limit (supplementary material Fig. S3). This result rules out the possibility that αvβ3 integrins affect the traction measurements on RGD-peptide-coated acrylamide gels.

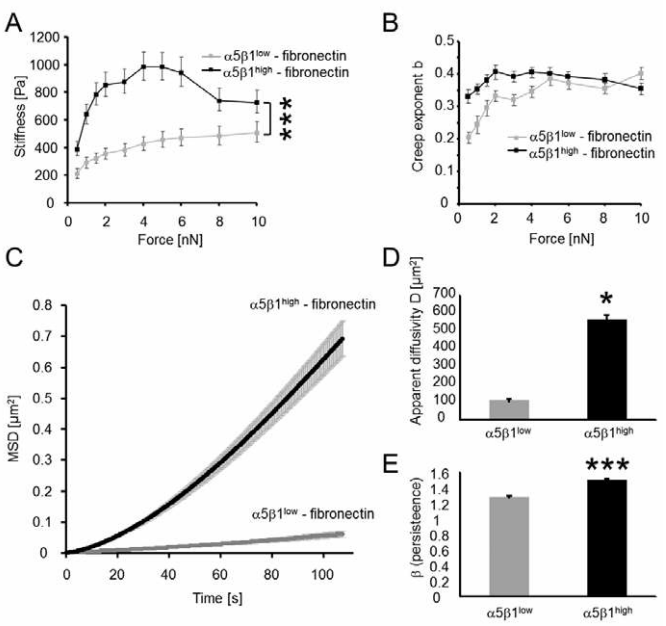

Fig. 7. Mechanical properties of α5β1^{high} and α5β1^{low} cells. (**A**) Stiffness of α5β1^{high} and α5β1^{low} cells measured during increasing force application to fibronectin-coated beads. (**B**) Power-law exponent *b* (cell fluidity) of α5β1^{high} and α5β1^{low} cells versus force applied to fibronectin-coated beads. The values are expressed as mean ± s.e.m. (**C–E**) MSD of spontaneous bead motion (C) showed a higher apparent diffusivity (D) and a higher persistence (power-law exponent β) (E) in α5β1^{high} cells than in α5β1^{low} cells. *$P<0.05$, ***$P<0.001$.

To characterize the contractile forces of each cell, the elastic strain energy stored in the polyacrylamide gel due to cell tractions was calculated as the product of local tractions and deformations, integrated over the spreading area of the cells (Butler et al., 2002). The strain energy of α5β1^{high} cells was sevenfold higher than that of α5β1^{low} cells (Fig. 8A,B). Even after normalization for differences in the spreading area, the strain energy of α5β1^{high} cells was still 3.5-fold higher than that of α5β1^{low} cells.

The addition of the myosin light chain kinase (MLCK) inhibitor ML-7 or the ROCK inhibitor Y27632 to α5β1^{high} cells reduced significantly ($P<0.001$) the percentage of invasive cells into 3D collagen matrices (Fig. 8D). In α5β1^{low} cells, only ML-7 but not Y27632 caused a small decrease in the percentage of invasive cells (Fig. 8D). The ROCK and MLCK inhibitors did not alter the invasion profile of α5β1^{low} cells, whereas both inhibitors reduced invasion of α5β1^{high} cells into deeper regions of the 3D collagen matrices (Fig. 8E,F). These effects were not caused by impaired cell adhesion because both subcell lines were still able to attach and spread on the surface of the 3D collagen matrices after addition of the inhibitors (Fig. 8C, top images). Furthermore, the inhibitors did not cause alterations in the cell morphology of invasive cells (Fig. 8C, bottom images). The addition of the actin polymerization inhibitor latrunculin B (2 μM) reduced the percentage of invasive α5β1^{high} cells and reduced their invasion depths, whereas the percentage of invasive α5β1^{low} cells and their invasion depths was not affected (Fig. 8G–I). These results indicate that α5β1^{high} cells are sensitive to changes in MLCK-mediated MLC phosphorylation and dephosphorylation and to acto-myosin contraction.

Subcell-line-specific dependence of cell invasion on MLC phosphorylation was further investigated by the addition of the serine/threonine phosphatase inhibitor calyculin A (1nM), which

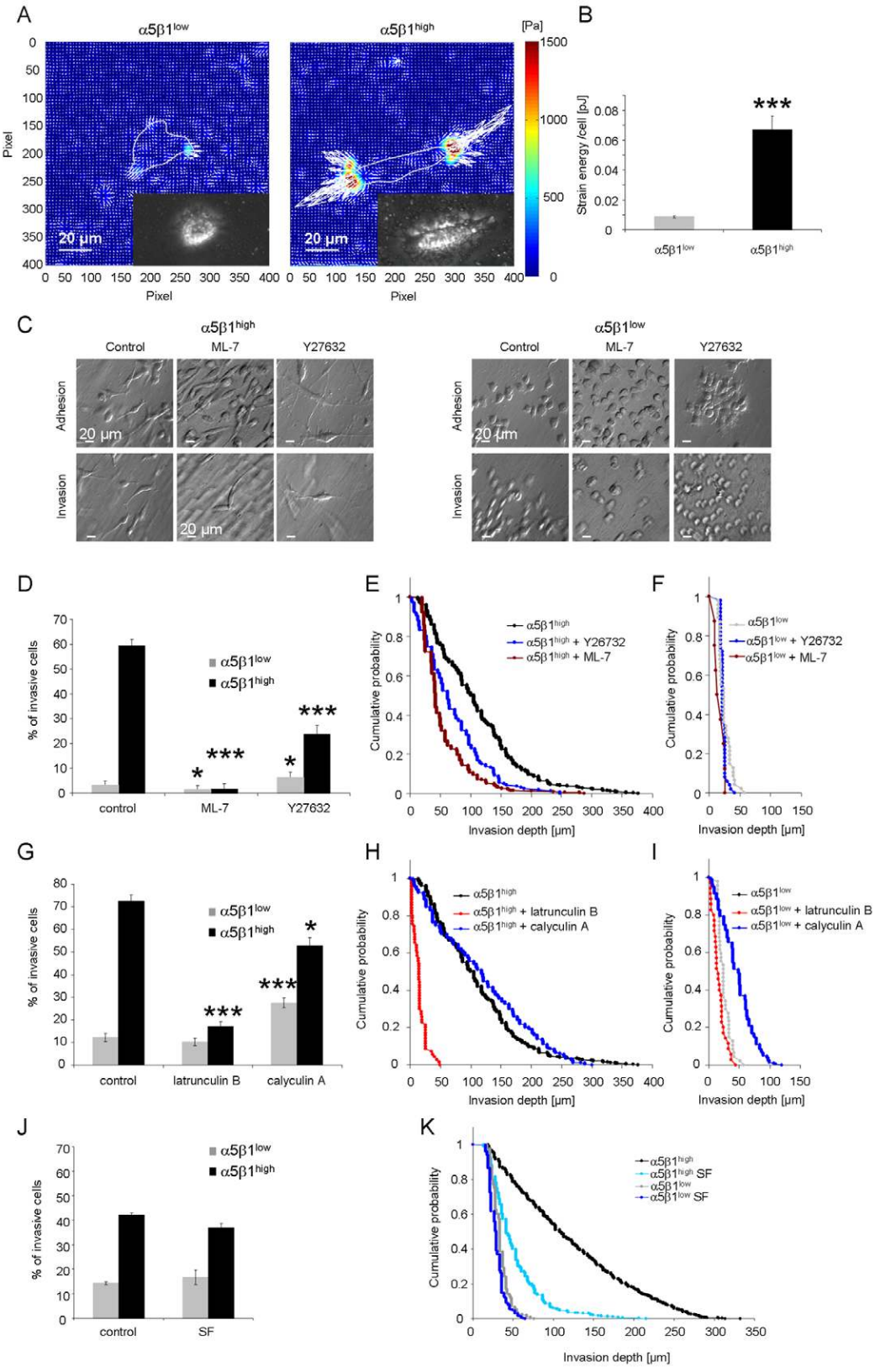

Fig. 8. Increased contractile force generation of α5β1^{high} cells and inhibition of contractile-force-mediated cell invasion. (**A**) Representative traction fields of a α5β1^{low} cell (left) and α5β1^{high} cell (right). The gray line represents the cell boundaries. The insets show a bright field image of the measured cells. (**B**) The strain energy per cell (mean + s.e.m.) of α5β1^{high} cells (n=80) was increased sevenfold compared to α5β1^{low} cells (n=84). (**C**) Modulation contrast images of adherent cells on top of collagen gels (top row) or after 3 days of gel invasion (bottom row) show no morphology changes after treatment with myosin contraction inhibitors ML-7 or Y27632. (**D**) Percentage (mean + s.e.m.) of invasive α5β1^{high} cells or α5β1^{low} cells determined after 3 days in the presence of 100 μM Y27632, 15 μM ML-7 or DMSO as control. (**E**,**F**) Invasion profiles of α5β1^{high} (E) and α5β1^{low} (F) cells treated with Y26732, ML-7 or DMSO as control. (**G**) Percentage of invasive cells (mean ± s.e.m.) of α5β1^{high} or α5β1^{low} cells was determined after 3 days in the presence of actin polymerization inhibitor (2 μM latrunculin B), myosin phosphatase inhibitor (1 nM calyculin A) or DMSO as control. (**H**,**I**) Invasion profiles of α5β1^{high} (H) and α5β1^{low} (I) cells treated with latrunculin B, calyculin A or DMSO as control. (**J**) The use of serum-free medium (SF) did not alter the percentage of invasive cells. (**K**) Serum-free conditions reduced the invasion depths of invasive α5β1^{high} cells but not α5β1^{low} cells. *P<0.05, ***P<0.001. Scale bars: 20 μm.

reduces the dephosphorylation of MLC and thereby increases contractility (Inutsuka et al., 2009). Calyculin A treatment increased the percentage of invasive α5β1^{low} cells and also increased their invasion depths but had little effect on α5β1^{high} cells (Fig. 8G–I). This indicates that an increase in contractility of α5β1^{low} cells enhances their invasiveness, whereas the contractility of α5β1^{high} cells was already at a level optimal for cell invasion and could not be further increased by calyculin A. Taken together, these data

demonstrate that the α5β1-integrin-mediated increased invasiveness is due to increased generation of contractile force.

Role of fibronectin in α5β1-integrin-mediated cell invasiveness

α5β1 integrins attach to 3D collagen fibers through the ECM protein fibronectin. The cell culture medium used in this study was supplemented with 10% fetal calf serum and contained substantial amounts of fibronectin. The percentage of invasive cells was not altered when serum-free medium was used (Fig. 8J); however, the invasion depth of $\alpha5\beta1^{high}$ cells but not $\alpha5\beta1^{low}$ cells was reduced (Fig. 8K). This suggests that the presence of fibronectin is important for α5β1-integrin-mediated cell invasion and leads to the question of whether $\alpha5\beta1^{high}$ cells secreted larger amounts of fibronectin.

Fibronectin concentration in the supernatant of MDA-MB-231, T24 and 786-O cancer cells selected for $\alpha5\beta1^{high}$, $\alpha5\beta1^{medium}$ and $\alpha5\beta1^{low}$ cells after 3 days of invasion into 3D collagen matrices was measured with ELISA. Cells were cultured initially in serum-free medium, but after 3 days of culture substantial amounts of fibronectin were secreted by all subcell lines with no significant differences between $\alpha5\beta1^{high}$ and $\alpha5\beta1^{low}$ cells (Fig. 9A). Similar results were obtained in MDA-MB-231 cells in which the α5 integrin subunit was knocked down with five different siRNA constructs (Fig. 9B). These results indicate that differences in the invasiveness of α5β1 subcell lines was not caused by differences in fibronectin secretion.

To test the effect of large concentrations of fibronectin, we added 0.1 mg/ml of fibronectin, RGD peptide, or vitronectin (which binds to α3β1 integrins) prior to the collagen polymerization step. Unbound matrix proteins or peptide were washed out before $\alpha5\beta1^{low}$ or $\alpha5\beta1^{high}$ cells were seeded onto the matrices. The presence of fibronectin or RGD peptide significantly enhanced the percentage of invasive $\alpha5\beta1^{low}$ and $\alpha5\beta1^{high}$ cells into 3D collagen matrices by 2.4- to 3.8-fold. We confirmed with confocal microscopy and immunofluorescence staining that the fibronectin was indeed incorporated into the collagen matrix (Fig. 9I). Furthermore, we found that under serum-free conditions the fibronectin staining of the 3D collagen matrix surrounding a cell was intensified (Fig. 9J, middle and right images), indicating that the invasive cells secrete fibronectin, and that this fibronectin associates with the 3D matrix. The presence of vitronectin, however, had no further invasion-enhancing effect (Fig. 9C,E,G). Together, these data confirm that the presence of the α5β1 integrin ligand fibronectin, or RGD peptide, in the matrix plays a key role for cell invasion. By contrast, the addition of soluble fibronectin or RGD peptide at the beginning of the invasion assay reduced the invasiveness of both $\alpha5\beta1^{high}$ and $\alpha5\beta1^{low}$ cells (Fig. 9K).

Effect of steric hindrance of the 3D collagen matrices on α5β1-integrin-facilitated cell invasion

We then tested the hypothesis that α5β1 integrin activation, stress fiber formation and contractile force generation is important for the cell to overcome the steric hindrance of the 3D collagen matrix. Hence, we expected that the invasion of $\alpha5\beta1^{low}$ cells would be more impaired by a higher steric hindrance of the matrix compared to $\alpha5\beta1^{high}$ cells. Steric hindrance was altered by changing the collagen concentration between 0.6 mg/ml and 5.8 mg/ml. The pore sizes of the collagen fiber network for some of the collagen concentrations have been previously measured (3.0 μm for 1.2 mg/ml; 1.3 μm for 2.4 mg/ml) (Mickel et al., 2008).

The invasion behavior of both subcell lines showed a biphasic response to alterations of collagen concentration. The percentage of invasive cells and their invasion depth was highest at an intermediate collagen concentration of 2.4 mg/ml. As expected, cell invasion was impaired at higher collagen concentrations. In particular, $\alpha5\beta1^{high}$ cells but not $\alpha5\beta1^{low}$ cells were able to invade a dense 5.8 mg/ml collagen matrix (Fig. 9D,F,H). These data support the hypothesis that integrin α5β1 facilitates cancer cell invasion through enhanced contractile forces that help the cells to overcome the steric hindrance of the ECM.

Interestingly, cell invasion was also impaired at lower collagen concentrations, whereby $\alpha5\beta1^{low}$ cells but not $\alpha5\beta1^{high}$ cells were able to invade into a loose 0.6 mg/ml collagen matrix (Fig. 9D,F,H). The reason for this diminished invasiveness is unclear and could be attributable to reduced ligand availability, but also to mechano-sensitive regulatory mechanisms in response to the low stiffness of loose 3D collagen matrices (Paszek et al., 2005; Pelham and Wang, 1997).

Discussion

Cancer cell invasion is a complex event and depends on the mechanical and biochemical properties of the microenvironment. Here, we demonstrate that increased expression of α5β1 integrins enhances tumor cell invasion into 3D collagen matrices through generation of a higher contractile force. We analyzed the surface expression of several integrins and integrin subunits of cancer cell lines with different invasive capabilities. In agreement with previous reports (Bauer et al., 2007), we found that the expression of αvβ3, α3 and α5 integrins were increased in invasive compared to non-invasive cancer cell lines. We focused in this study on the mechanism that leads to higher invasiveness of cells with high α5β1 integrin expression.

The mechanisms promoting cancer cell invasion are only fragmentarily investigated, but there is general agreement that biomechanical factors determine the speed of cell migration in dense 3D collagen matrices (Friedl and Brocker, 2000; Mierke et al., 2008b; Zaman et al., 2006). These factors include adhesion forces, degradation of the ECM through secretion of matrix-degrading enzymes, cytoskeletal dynamics, cellular stiffness and fluidity, and contractile force generation (Mierke, 2008; Mierke et al., 2008b; Wolf et al., 2003; Zaman et al., 2006). To investigate which of these biomechanical factors contribute to the higher invasiveness of cells with high α5β1 integrin expression, we isolated subcell lines with high and low α5β1 integrin expression from MDA-MB-231 breast cancer cells, T24 bladder and 786-O kidney cancer cells. In each case we found that $\alpha5\beta1^{high}$ cells were highly invasive. Because it is likely that the selection for α5β1 integrins causes changes in the levels of co-regulated proteins, we confirmed a specific involvement of α5β1 integrins and showed that the addition of blocking anti-α5 or anti-β1 integrin antibodies to $\alpha5\beta1^{high}$ cells as well as α5-integrin-specific knockdown dramatically decreased the invasiveness into 3D ECMs. Expression levels of α1 and α2 integrin subunits were also increased in $\alpha5\beta1^{high}$ cells, but the effect of anti-α1 and anti-α2 blocking antibodies or α1- and α2-integrin-specific knockdown on cell invasiveness was smaller than the effect of α5 blocking or specific knockdown. Decreased availability of matrix-bound fibronectin, the main α5β1 integrin ligand, and addition of soluble fibronectin lead to reduced cell invasiveness, whereas the addition of matrix-bound fibronectin leads to increased cell invasiveness. These results indicate that α2β1 integrins, and especially α5β1 integrins, play a key role for cell invasion into 3D ECMs.

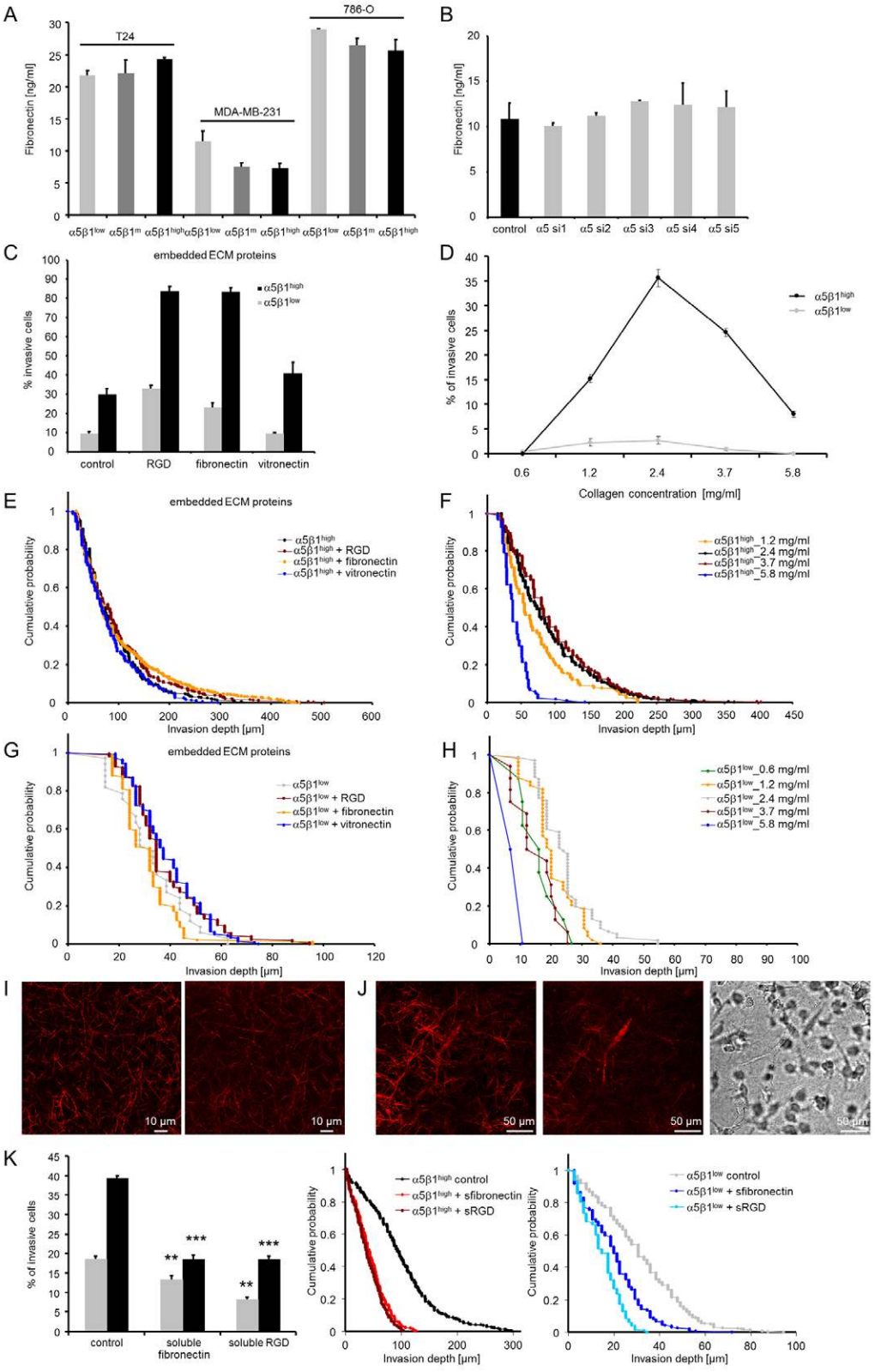

Fig. 9. Effect of ECM proteins and collagen density on α5β1-integrin-facilitated cell invasion.
(**A**) Concentration of fibronectin in the medium secreted by T24, MDA-MB-231 and 786-O cancer cells with low, medium and high α5β1 integrin expression after 3 days of invasion into 3D collagen matrices. (**B**) Concentration of secreted fibronectin in the medium after 3 days of siRNA-mediated knockdown of α5 integrin. Unspecific siRNA served as control and five different siRNAs were used for specific α5 knockdown (α5 si1–si5). (**C**) The percentage of invasive cells strongly increased in 3D matrices containing 100 μg/ml fibronectin (embedded) or RGD peptide (embedded), and slightly increased in 3D matrices containing 100 μg/ml vitronectin (embedded). (**D**) Five different collagen concentrations of 0.6, 1.2, 2.4, 3.7, and 5.8 mg/ml were tested for cell invasion. After 3 days, $\alpha5\beta1^{high}$ cells were able to invade into 1.2–5.8 mg/ml collagen gels, whereas $\alpha5\beta1^{low}$ cells were able to migrate into 0.6–3.7 mg/ml collagen gels. (**E**–**H**) The invasion profiles of $\alpha5\beta1^{high}$ (E) and $\alpha5\beta1^{low}$ (G) cells were not altered by the addition of fibronectin, RGD peptide or vitronectin. Invasion profiles of $\alpha5\beta1^{high}$ (F) and $\alpha5\beta1^{low}$ (H) cells in 3D ECMs with increasing collagen concentrations, as indicated. (**I**) Confocal images of 3D fibronectin–collagen matrices. Left: reflection mode shows the collagen fibers. Right: fluorescent image of an anti-fibronectin staining of the same matrix. (**J**) Confocal images of a 3D collagen matrix with an invasive $\alpha5\beta1^{high}$ cell. Left: reflection mode shows the matrix fibers and the cell. Middle: fibronectin staining of the same matrix and the cell. Right: bright field image of the same field of view. (**K**) Left: the percentage of invasive $\alpha5\beta1^{high}$ and $\alpha5\beta1^{low}$ cells strongly decreased in 3D matrices containing 100 μg/ml soluble fibronectin or 100 μg/ml soluble RGD peptide. The invasion profiles of $\alpha5\beta1^{high}$ (middle) and $\alpha5\beta1^{low}$ cells (right) show reduced invasiveness after addition of soluble (s) fibronectin and RGD peptide. The bar graphs show means + s.e.m. $^{**}P<0.01$, $^{***}P<0.001$.

We further showed that the enhanced invasiveness of $\alpha5\beta1^{high}$ cells was not mediated through differences in fibronectin secretion or proteolytic enzyme activity. Rather, we observed increased cell spreading, focal adhesion density and stress fiber formation in $\alpha5\beta1^{high}$ cells. These morphological changes were accompanied by increased stiffness, cytoskeletal remodeling dynamics and contractile force generation.

The signal transduction pathways that connect integrin adhesion events with traction force generation and cell invasion are still elusive, although important components have been studied in detail,

such as the activation of α5β1 integrins by ECM ligands (Friedland et al., 2009; Huveneers et al., 2008), the formation of focal adhesions following integrin activation (Burridge and Wennerberg, 2004), the connection between focal adhesion assembly and contractile forces (Balaban et al., 2001; Friedland et al., 2009; Gallant et al., 2005), and the connection between contractile forces and 3D cell invasion (Mierke et al., 2008c; Rösel et al., 2008). Here, we show that increased expression and activation of α5β1 integrins leads to increased adhesion forces, increased focal adhesion assembly, increased stress fiber formation and increased contractile forces that ultimately help the cell to overcome the steric hindrance of the ECM. The details of the mechanisms by which α5β1 integrins regulate increased contractile activation or stress fiber formation are not clear but could be partly mediated by growth factor signaling because ERK1/2 inhibition was found to greatly reduce the invasiveness of $\alpha5\beta1^{high}$ cells.

A fraction of $\alpha5\beta1^{low}$ cells remained weakly invasive, presumably through an invasion mode that differed from those of $\alpha5\beta1^{high}$ cells. For instance, blocking myosin contraction through the MLCK inhibitor ML-7 or the ROCK inhibitor Y27632 did not further diminish the invasion $\alpha5\beta1^{low}$ cells. These results suggest that $\alpha5\beta1^{low}$ cells can employ invasion strategies that do not rely on the generation of contractile forces. Nonetheless, by increasing the contractility of $\alpha5\beta1^{low}$ cells using calyculin A, they show increased invasion.

In conclusion, we have identified and isolated subpopulations within cancer lines that show increased invasiveness into 3D collagen matrices. These subpopulations are characterized by high expression of α5β1 integrins that facilitate the generation of contractile forces and enhance the invasiveness into 3D collagen matrices. Moreover, the fact that we were able to isolate long-term-stable, highly invasive subpopulations from parental cancer cells suggests that these subpopulations have a particularly high potential to metastasize. We speculate that a similar selection process towards high α5β1 integrin expression might also take place during the early stages of tumor spreading that accelerates the transformation from a benign to a malign tumor. We conclude that the generation of contractile forces is the driving factor for increased α5β1-integrin-mediated cell invasion into 3D ECMs, and propose that the measurement of biomechanical properties might be a prognostic parameter for determining the malignancy of tumors.

Materials and Methods

Cell culture

Human cancer lines from colon (13), breast (13), skin (5), lung (4), prostate (2), pancreas (2), bladder (3), kidney (2), cervix (4), hypo pharynx (1), vulva (1) and brain (1) were purchased from ATCC-LGC-Promochem (Wesel, Germany) (see supplementary material Table S1). Cancer cells were maintained in low-glucose (1 g/l) DMEM supplemented with 10% FCS (low endotoxin,<0.1 EU/ml), 2 mM L-glutamine and 100U/ml penicillin–streptomycin (Biochrom, Berlin, Germany). 80%-confluent cells were used in passages 5–30. Accutase was used for cell harvesting (<1% dead cells). Mycoplasma contamination was excluded using a Mycoplasma detection kit (Roche, Mannheim, Germany). All other chemicals used were purchased from Sigma (Taufkirchen, Germany).

Cell invasion assay

For the preparation of 5.8 mg/ml 3D collagen matrices, 0.775 ml collagen-R (2 mg/ml rat collagen type I; Serva, Heidelberg, Germany), 1.95 ml collagen-R (10.68 mg/ml rat collagen type I; Becton Dickinson, Heidelberg, Germany), and 0.775 collagen-G (4 mg/ml bovine collagen type I; Biochrom) were mixed. After addition of 0.4 ml $NaHCO_3$ buffer (26.5 mM) and 0.4 ml 10× DMEM, the mixture was neutralized using 130 µl 1N NaOH, pipetted into 3.5-cm dishes and polymerized at 37°C, 5% CO_2 and 95% humidity for 2 hours. The 3D collagen matrices were incubated overnight with 2 ml DMEM (Mierke et al., 2008c). Other matrices with lower collagen concentrations (0.6, 1.2, 2.4 and 3.7 mg/ml) were obtained by dilution of the non-polymerized 5.8 mg/ml collagen mixture with PBS buffer and 10× DMEM. 100,000 cancer cells were seeded on top of the 3D collagen matrices and cultured for 72 hours at 37°C, 5% CO_2 and 95% humidity in DMEM containing 10% FCS. At this time period, differences in the invasiveness of cells were clearly visible. Non-invasive cells could be readily identified by their nuclei, which were located in one layer that coincided with the location of the topmost collagen fibers. A cell was counted as invasive when its nucleus was located below the layer formed by the non-invasive cells. Because of the depth of field of a 40× 0.6 NA objective, the uncertainty of this method was approximately 5 µm. These 3D ECM matrices also contained fibronectin sequestered from the fetal calf serum in the medium, and fibronectin secreted from the cancer cells (see also confocal images, Fig. 9I). Because fibronectin is the main ligand for α5β1 integrins, the matrices are suitable for analyzing α5β1-dependent cell behavior. To analyze the function of integrin ligands in more detail, 3D collagen matrices were also polymerized in the presence of 100 µg/ml of fibronectin, RGD peptide or vitronectin. For serum-free cell invasion, cells were cultured 24 hours before and during the invasion assay in EX-cell293 medium (SAFCBiosciences, Lenexa, Kansas) with 100 U/ml penicillin–streptomycin. After fixation with 2.5% glutaraldehyde solution in PBS buffer, the percentage of invasive cells and their invasion depths were determined in 12 randomly selected fields of view. To determine the percentage of invasive cells, the adherent cells on top of the 3D collagen matrices were also counted. The invasion profile plots only contain the invasive cells. The percentage of cells that did not invade is given in the bar graphs.

In Fig. 2, the separation into invasive and non-invasive cell lines was based on invasion scores that were defined as invasion depth multiplied by cell number density per 1 mm^2 (Mierke et al., 2008c).

The aspect ratio of cells was determined after 3 days of cell invasion into 2.4 mg/ml 3D collagen matrices. We first identify the optical section through an invasive cell that showed the largest cell dimension in the x–y plane. From that image, we calculated the aspect ratio as the distance between the two points on the cell outline with the largest separation (long axis), divided by the largest cell dimension found anywhere perpendicular to the long axis.

Migration speed and mean squared displacement

Some 10,000 $\alpha5\beta1^{low}$ or $\alpha5\beta1^{high}$ cells were seeded into collagen gels before polymerization. The matrices with embedded cells were treated as described above. Cell movements were computed from phase-contrast images recorded with 10× magnification using a Fourier-based difference-with-interpolation algorithm (Raupach et al., 2007). The MSD of cell movements with time t was described with a power-law relationship $MSD=D(t/t_0)^{\beta}$ (Dieterich et al., 2008; Oakes et al., 2009; Potdar et al., 2010), where t_0 is the time interval of the image recordings (1 minute), D is the apparent diffusion coefficient, and the power-law exponent β is a measure of persistence, with β~1 for randomly and β~2 for ballistically migrating cells (Raupach et al., 2007). The average migration speed over any time period can be obtained from the square root of the MSD. The MSD of tumor cells reveals that the migration process is not a Brownian random walk but is superdiffusive due to directional persistence and temporal fluctuations in migration speed.

ELISA

Supernatant from 100,000 cells of each subcell line was collected after 3 days of cell invasion. Fibronectin concentrations were determined using a Fibronectin-Elisa Kit according to the manufacturer's instructions (R&D systems).

Flow cytometry

80%-confluent cells were harvested and resuspended in HEPES-buffer (20 mM HEPES, 125 mM NaCl, 45 mM glucose, 5 mM KCl, 0.1% albumin, pH 7.4). Cells were incubated with mouse antibodies against human integrins α1 (FB12), α2 (P1E6), α3 (17C6; Biozol), α4 (P1H4), α5 (Biozol), α6 (MP4F10; R&D), β1 (Biozol), αvβ3 (LM609), β4 (R&D) and αvβ5 (P1F6), and against human MT1-MMP (128527; R&D) and MMP-7 (111433; R&D), all purchased from Millipore (Temecula, CA) unless otherwise stated. Isotype-matched antibodies were used as controls (Caltag, Burlingame, CA). After 30 minutes at 4°C, cells were washed and stained with a R-phycoerythrin-labeled goat anti-mouse-IgG [$F(ab)_2$-fragment; Dianova]. Flow cytometry was performed using a FACSCalibur System (BectonDickinson, Heidelberg, Germany).

Isolation of tumor cell variants

Tumor cell variants with high, medium and low α5β1 integrin expression were isolated from parental MDA-MB-231 (breast), 786-O (kidney) and T24 (bladder) cancer cells using a cell sorter, and single cells were plated into 96-well plates. Cells were expanded, and the expression of α5 integrin was measured by flow cytometry. Repeated measurements of the cell surface expression of α5β1 integrin confirmed that the α5β1 expression phenotype of the subcell lines remained stable for at least 100 generations (supplementary material Fig. S1).

siRNA transfection

Some 200,000 80%-confluent $\alpha5\beta1^{high}$ cells were seeded into 3.5-cm dishes and cultured in 2 ml DMEM complete medium. 5 µl of a solution containing 20 µM α5 integrin (target sequences were: nr.1, 5′-CCCATTGAATTTGACAGCAAA-3′; nr.2,

5′-TGGGCCAACAAAGAACACTAA-3′; nr.3, 5′-CAGCCCAGAGACATACTT-GAA-3′; nr.4, 5′-AATCCTTAATGGCTCAGACAT-3′; and nr.5, 5′-CAGGG-TCTACGTCTACCTGCA-3′), α1-integrin (5′-TTGGACTTTAATCTTACCGAT-3′), α2-integrin (nr.1, 5′-TCGCTAGTATTCCAACAGAAA-3′ and nr.2, 5′-CCCGA-GCACATCATTTATATA-3′) or Allstar control RNAi solution (control siRNA), 12 µl HiPerFect-Reagent (Qiagen) and 100 µl DMEM were mixed (Mierke et al., 2008c). RNAi-mediated α5, α1 and α2 integrin knockdowns were confirmed by flow cytometry using anti-α5-integrin, anti-α1 integrin or anti-α2 integrin and Cy_2-labeled anti-mouse-IgG antibodies (Dianova). Transfection efficiency was determined by flow cytometry to be >99% using 20 µM Alexa-Fluor-546-labeled siRNA.

Modulation of cell invasion

To inhibit or modulate cell invasion, we added 15 µM ML-7 (Calbiochem), 100 µM Y27632 (Sigma), 2 µM latrunculin B (Sigma), 1 nM calyculin A (Calbiochem) or 10–20 µM ERK inhibitor 328005 (Calbiochem) to the collagen invasion assay prior to cell seeding. The effect of integrins on cell invasion was analyzed in the presence or absence of 100 µl of blocking (inhibitory) antibodies for integrins α5 (MAB1956Z clone P1D6, Millipore), β1 (MAB2253Z clone 6S6, Millipore), α1 (MAB1973Z clone FB12, Millipore) and α2 (MAB1950Z clone P1E6, Millipore). An isotype-matched antibody served as control (Millipore).

Inhibition of enzymatic degradation

To inhibit enzymatic degradation of the 3D collagen matrices, we added a protease inhibitor cocktail (PI) before the start of the invasion assay. The PI cocktail contained 50 µM GM6001 (broad spectrum matrix-metalloproteinase inhibitor), 250 µM E-64, 2 µM Leupeptin, 100 µM PepstatinA and 2.2 µM Aprotinin (all from Calbiochem) (Bloom et al., 2008; McNulty et al., 2009; Wolf et al., 2003).

Immunofluorescence

Some 20,000 cells were seeded onto glass cover slips (Menzel, Braunschweig, Germany) coated with 50 mg/ml collagen type I, 50 µg/ml fibronectin (Roche), 50 µg/ml RGD peptide (Ac-Gly-D-Arg-Gly-Asp-Ser-Pro-Ala-Ser-Ser-Lys-(Gly)4-Ser-D-Arg-(Leu)6-D-Arg-NH_2; Peptides International, Louisville, KY) or 5 mg/ml vitronectin for 2 hours at 37°C. After 24 hours, cells were fixed using 3% PFA (15 minutes at 20°C), permeabilized for 5 minutes with 0.1% Triton X-100, stained for 30 minutes at 20°C with antibodies (1:200) against vinculin, or paxillin (Chemicon), and subsequently stained with Cy2-labeled antibody and 66 nM Alexa-Fluor-546–phalloidin (MolecularProbes, Eugene, Oregon). After Hoechst-33342 staining (5 minutes at 20°C), cells were embedded in Mowiol. 10–20 fields of view (20× or 40× magnification) were recorded randomly. Spreading area was computed using a custom image analysis software written in MATLAB. The number of focal adhesions per cell was determined from paxillin-stained cells using a custom image analysis program. Images were high-pass filtered, and focal adhesions were detected and counted when the fluorescence intensity of connected pixels over an area of at least 0.5 μm^2 was above a fixed threshold.

For confocal microscopy, the cells and 3D matrices were stained with a fibronectin anti-human antibody (1:200; Sigma) for 60 minutes at 20°C and then with a R-phycoerythrin-labeled goat anti-mouse-IgG antibody ($F(ab)_2$-fragment, 1:200; Dianova) for 60 minutes at 20°C. The confocal images were taken with a confocal microscope (Leica TCS SP5 II) equipped with a water immersion 20× 1.00NA objective.

Magnetic tweezers

Using magnetic-tweezers, step-forces ranging from 0.5 to 10 nN were applied to superparamagnetic epoxylated 4.5 µm beads coated with collagen (100 µg/ml), RGD peptide (50 µg/ml), fibronectin (100 µg/ml and 50 µg/ml) or anti-α5-antibody (5 µg/ml) (Kollmannsberger and Fabry, 2007; Mierke et al., 2008a; Mierke et al., 2008c). 2×10^5 beads were sonicated, added to 10^5 cells, and incubated for 30 minutes at 37°C and 5% CO_2. Measurements were performed at 37°C with an inverted microscope (DMI-Leica). The creep response $J(t)$ of cells during force application followed a power law in time, $J(t)=a(t/t_0)^b$, where the pre-factor a and the power-law exponent b were force-dependent, and the reference time t_0 was set to 1 second. Bead displacement in response to a staircase-like force followed a superposition of power laws (Hildebrandt, 1969) from which the force-dependence of a and b was determined by a least-squares fit (Mierke et al., 2008a). The parameter a (units are micrometers per nanoNewton) characterizes the elastic cell properties and corresponds to a compliance (inverse of stiffness) (Mierke et al., 2008a).

The force–distance relationship (units are nanoNewtons per micrometer) is related to cell stiffness (units are Pascals) by a geometric factor that depends on the contact area between the bead and the cell (or the degree of bead internalization) and the cell height. If those parameters are known, e.g. from scanning electron micrographs (Fig. 6J,K), the geometric factor can be estimated from a finite element analysis (Mijailovich et al., 2002). Without knowledge of cell height and bead internalization, one can still estimate the typical strain ε as the bead displacement d divided by the bead radius r, and the typical stress σ as the applied force F divided by the bead cross-sectional area πr^2 such that the cell stiffness $G=\sigma/\varepsilon=r/d\times F/(\pi r^2)$ (Kasza et al., 2009). For the 4.5 µm beads as used in our study, the geometric factor is 0.14 μm^{-1}, and a cell with an apparent stiffness of 1 nN/µm would have a ‘proper’ stiffness of 140 Pa (Fig. 7A).

The power-law-exponent b reflects the stability of force-bearing cellular structures connected to the beads. A value for b=1 and b=0 indicates Newtonian-viscous and elastic behavior, respectively (Fabry et al., 2001). A non-zero power-law exponent implies that part of the deformation energy during magnetic force application is not elastically stored in the cytoskeleton but is dissipated in the form of heat because of remodeling of the cytoskeletal structures to which the beads are connected (Kollmannsberger and Fabry, 2009). Hence, dissipation is directly linked to the rate at which the elastic bonds in the cytoskeleton break up and turn over. The turn-over of acto-myosin bonds also contributes to the dissipative properties (Fredberg et al., 1996) and, although this is not considered a remodeling event, it enables contractility-driven shape changes in the cytoskeleton.

Adhesion strength

Some 50,000–100,000 cells were seeded in 3.5-cm dishes. After 1 day, the cells were incubated with beads coated with ECM protein or antibody for 30 minutes at 37°C, 5% CO_2, and 95% humidity. The detachment of beads coated with fibronectin, RGD peptide, collagen type I or anti-α5-antibody from the cells was measured during force application ranging from 0.5 to 10 nN. We then recorded the minimum force at which the beads detached from the cells. The percentage of detached beads in relation to the detachment force was used to quantify the bead binding strength to the cell.

We validated the ability of the method to specifically measure integrin-mediated adhesion forces by blocking β1 integrin receptors with a blocking antibody (10 µg/ml, MAB2253Z clone 6S6; Millipore) prior to addition of fibronectin beads, and found significantly decreased rupture forces. Furthermore, we added soluble fibronectin prior to addition of beads coated with fibronectin, RGD peptide or anti-α5-antibody, or we added soluble collagen type I prior to addition of beads coated with collagen type I. In all cases, the detachment forces were strongly decreased (supplementary material Table S2).

Spontaneous bead diffusion

Some 300,000 cells were seeded into 3.5-cm dishes containing CO_2-independent media and were cultured overnight at 37°C, 5% CO_2 and 95% humidity. After incubation with fibronectin- or RGD-peptide-coated beads for 30 minutes at 37°C, 5% CO_2 and 95% humidity, the position of beads was tracked over 5 minutes. The beads moved spontaneously, with a MSD that also followed a power law with time, $MSD=D(t/t_0)^\beta+c$. The evolution of the MSD over time, t, can be described by an apparent diffusivity, D, and the persistence of motion can be described, by the power-law exponent β. The additive term c reflects random noise from thermal and non-thermal sources such as single myosin motors, and t_0 was arbitrarily set to 1 second. The fit parameters were determined by a least-squares fit (Raupach et al., 2007). Measurements of the spontaneous bead movements were performed after at least 30 minutes of bead binding, which is sufficient to connect the beads to the cytoskeleton. The details of the connection matter little and do not influence the bead motion once the beads are firmly connected to the cytoskeleton (Metzner et al., 2010).

Traction microscopy

Acrylamide (4.7%)–bis-acrylamide (0.24%) gels were casted on non-electrostatic silane-coated glass slides (Pelham and Wang, 1997). The Young’s modulus of the gels was 5.4 kPa. Yellow-green fluorescent 0.5 µm carboxylated beads (Invitrogen) were embedded in the gels and centrifuged (300 ***g***) towards the gel surface during polymerization at 4°C (Mierke et al., 2008a; Mierke et al., 2008c). The beads served as markers for gel deformations. The gel surface was activated with sulfo-SANPAH (Pierce, Bonn, Germany) and coated with 50 µg/ml RGD peptide.

FACS analysis showed that the expression of αvβ3 integrins on the two subcell lines was below the detection limit. This ruled out the possibility that the αvβ3 integrins affect the traction measurements on RGD-coated acrylamide gels (supplementary material Fig. S4).

After cells adhered to the gels, cell tractions were computed from the gel surface displacements measured before and after force relaxation and detachment of cells with 8 µM cytochalasin-D and 15 µM ML-7 in trypsin/EDTA (Butler et al., 2002). Gel deformations were measured using a Fourier-based difference-with-interpolation image analysis (Raupach et al., 2007). The experiments were performed at 37°C, 5% CO_2 and 95% humidity in DMEM containing 10% FCS in a microscope stage incubation chamber.

Transmission electron microscopy

Cells were fixed in 4% PFA and 0.1% glutaraldehyde, postfixed in 2% buffered osmium tetroxide, dehydrated through a graded ethanol series and embedded in epoxy resin. For orientation, 1.0-µm sections were stained with toluidine blue. Ultrathin sections of 70 nm were stained with uranyl acetate, lead citrate and examined by transmission electron microscopy (TEM) (EM906E; Zeiss, Oberkochen, Germany).

Scanning electron microscopy and bead internalization

2.5% glutaraldehyde-fixed cells in 3D collagen matrices were dehydrated with an ethanol series, washed with hexadimethylsilazane reagent (Electron-Microscopy-Science, Hatfield, PA) and air-dried (Mierke et al., 2008c). After sputter-coating with gold, cells were analyzed using scanning electron microscopy (SEM) (ISI-SX-40,

International Scientific Instruments, Milpitas, CA). Cells were incubated with beads coated with 50 μg/ml RGD peptide for 30 minutes, and the percentage of internalized beads determined.

Statistical analysis

Data were expressed as mean values ± s.e.m. Statistical analysis was performed using the Student's *t*-test. $P<0.05$ was considered significant.

We thank Ursula Schlötzer-Schrehardt for help with TEM, Philip Kollmannsberger for help with the magnetic tweezer experiments, Robert Schmiedl for help with the SEM, Wolfgang H. Goldmann for helpful discussions, Ulrike Scholz for secretarial assistance, and Barbara Reischl, Christine Albert and Werner Schneider for technical assistance. This work was supported by Deutsche Forschungsgemeinschaft (FA336/2-2, SFB643, and a 'cluster of excellence' grant 'Engineering of Advanced Materials'), Deutsche Krebshilfe (107384 and 109432), European Commissions (TPA4 FP6), National Institutes of Health grant NIH-HL65960, the Thomas-Wildey-Institut e.V., an ELAN grant of the University of Erlangen-Nuremberg, and an intramural grant of the IZKF. Deposited in PMC for release after 12 months.

Supplementary material available online at
http://jcs.biologists.org/cgi/content/full/124/3/369/DC1

References

Al-Mehdi, A. B., Tozawa, K., Fisher, A. B., Shientag, L., Lee, A. and Muschel, R. J. (2000). Intravascular origin of metastasis from the proliferation of endothelium-attached tumor cells: a new model for metastasis. *Nat. Med.* **6**, 100-102.

Balaban, N. Q., Schwarz, U. S., Riveline, D., Goichberg, P., Tzur, G., Sabanay, I., Mahalu, D., Safran, S., Bershadsky, A., Addadi, L. et al. (2001). Force and focal adhesion assembly: a close relationship studied using elastic micropatterned substrates. *Nat. Cell Biol.* **3**, 466-472.

Batlle, E., Sancho, E., Franci, C., Dominguez, D., Monfar, M., Baulida, J. and Garcia De Herreros, A. (2000). The transcription factor snail is a repressor of E-cadherin gene expression in epithelial tumour cells. *Nat. Cell Biol.* **2**, 84-89.

Bauer, K., Mierke, C. and Behrens, J. (2007). Expression profiling reveals genes associated with transendothelial migration of tumor cells: a functional role for alpha v beta3 integrin. *Int. J. Cancer* **121**, 1910-1918.

Behrens, J., Mareel, M. M., Van Roy, F. M. and Birchmeier, W. (1989). Dissecting tumor cell invasion: epithelial cells acquire invasive properties after the loss of uvomorulin-mediated cell-cell adhesion. *J. Cell Biol.* **108**, 2435-2447.

Bloom, R. J., George, J. P., Celedon, A., Sun, S. X. and Wirtz, D. (2008). Mapping local matrix remodeling induced by a migrating tumor cell using 3-D multiple-particle tracking. *Biophys. J.* **95**, 4077-4088.

Buckley, C. D., Doyonnas, R., Newton, J. P., Blystone, S. D., Brown, E. J., Watt, S. M. and Simmons, D. L. (1996). Identification of alpha v beta 3 as a heterotypic ligand for CD31/PECAM-1. *J. Cell Sci.* **109**, 437-445.

Burridge, K. and Wennerberg, K. (2004). Rho and Rac take center stage. *Cell* **116**, 167-179.

Butler, J. P., Tolic-Norrelykke, I. M., Fabry, B. and Fredberg, J. J. (2002). Traction fields, moments, and strain energy that cells exert on their surroundings. *Am. J. Physiol. Cell Physiol.* **282**, C595-C605.

Cano, A., Perez-Moreno, M. A., Rodrigo, I., Locascio, A., Blanco, M. J., del Barrio, M. G., Portillo, F. and Nieto, M. A. (2000). The transcription factor snail controls epithelial-mesenchymal transitions by repressing E-cadherin expression. *Nat. Cell Biol.* **2**, 76-83.

Caswell, P. T., Spence, H. J., Parsons, M., White, D. P., Clark, K., Cheng, K. W., Mills, G. B., Humphries, M. J., Messent, A. J., Anderson, K. I. et al. (2007). Rab25 associates with alpha5beta1 integrin to promote invasive migration in 3D microenvironments. *Dev. Cell* **13**, 496-510.

Caswell, P. T., Chan, M., Lindsay, A. J., McCaffrey, M. W., Boettiger, D. and Norman, J. C. (2008). Rab-coupling protein coordinates recycling of alpha5beta1 integrin and EGFR1 to promote cell migration in 3D microenvironments. *J. Cell Biol.* **183**, 143-155.

Damsky, C. H., Knudsen, K. A., Bradley, D., Buck, C. A. and Horwitz, A. F. (1985). Distribution of the cell substratum attachment (CSAT) antigen on myogenic and fibroblastic cells in culture. *J. Cell Biol.* **100**, 1528-1539.

Danen, E. H., van Rheenen, J., Franken, W., Huveneers, S., Sonneveld, P., Jalink, K. and Sonnenberg, A. (2005). Integrins control motile strategy through a Rho-cofilin pathway. *J. Cell Biol.* **169**, 515-526.

De Craene, B., Gilbert, B., Stove, C., Bruyneel, E., van Roy, F. and Berx, G. (2005). The transcription factor snail induces tumor cell invasion through modulation of the epithelial cell differentiation program. *Cancer Res.* **65**, 6237-6244.

Dieterich, P., Klages, R., Preuss, R. and Schwab, A. (2008). Anomalous dynamics of cell migration. *Proc. Natl. Acad. Sci. USA* **105**, 459-463.

Elson, E. L. (1988). Cellular mechanics as an indicator of cytoskeletal structure and function. *Annu. Rev. Biophys. Biophys. Chem.* **17**, 397-430.

Fabry, B., Maksym, G. N., Butler, J. P., Glogauer, M., Navajas, D. and Fredberg, J. J. (2001). Scaling the microrheology of living cells. *Phys. Rev. Lett.* **87**, 148102.

Festuccia, C., Angelucci, A., Gravina, G. L., Biordi, L., Millimaggi, D., Muzi, P., Vicentini, C. and Bologna, M. (2005). Epidermal growth factor modulates prostate cancer cell invasiveness regulating urokinase-type plasminogen activator activity. EGF-receptor inhibition may prevent tumor cell dissemination. *Thromb. Haemost.* **93**, 964-975.

Fredberg, J. J., Jones, K. A., Nathan, M., Raboudi, S., Prakash, Y. S., Shore, S. A., Butler, J. P. and Sieck, G. C. (1996). Friction in airway smooth muscle: mechanism, latch, and implications in asthma. *J. Appl. Physiol.* **81**, 2703-2712.

Friedl, P. and Brocker, E. B. (2000). The biology of cell locomotion within three-dimensional extracellular matrix. *Cell. Mol. Life Sci.* **57**, 41-64.

Friedland, J. C., Lee, M. H. and Boettiger, D. (2009). Mechanically activated integrin switch controls alpha5beta1 function. *Science* **323**, 642-644.

Frixen, U. H., Behrens, J., Sachs, M., Eberle, G., Voss, B., Warda, A., Lochner, D. and Birchmeier, W. (1991). E-cadherin-mediated cell-cell adhesion prevents invasiveness of human carcinoma cells. *J. Cell Biol.* **113**, 173-185.

Gallant, N. D., Michael, K. E. and Garcia, A. J. (2005). Cell adhesion strengthening: contributions of adhesive area, integrin binding, and focal adhesion assembly. *Mol. Biol. Cell* **16**, 4329-4340.

Geiger, B., Bershadsky, A., Pankov, R. and Yamada, K. M. (2001). Transmembrane crosstalk between the extracellular matrix-cytoskeleton crosstalk. *Nat. Rev. Mol. Cell Biol.* **2**, 793-805.

Giannone, G. and Sheetz, M. P. (2006). Substrate rigidity and force define form through tyrosine phosphatase and kinase pathways. *Trends Cell. Biol.* **16**, 213-223.

Gilcrease, M. Z., Zhou, X., Lu, X., Woodward, W. A., Hall, B. E. and Morrissey, P. J. (2009). Alpha6beta4 integrin crosslinking induces EGFR clustering and promotes EGF-mediated Rho activation in breast cancer. *J. Exp. Clin. Cancer Res.* **28**, 67.

Hemler, M. E., Huang, C. and Schwarz, L. (1987). The VLA protein family. Characterization of five distinct cell surface heterodimers each with a common 130,000 molecular weight beta subunit. *J. Biol. Chem.* **262**, 3300-3309.

Hildebrandt, J. (1969). Comparison of mathematical models for cat lung and viscoelastic balloon derived by Laplace transform methods from pressure-volume data. *Bull. Math. Biophys.* **31**, 651-667.

Huveneers, S., Truong, H., Fassler, R., Sonnenberg, A. and Danen, E. H. (2008). Binding of soluble fibronectin to integrin alpha5 beta1-link to focal adhesion redistribution and contractile shape. *J. Cell Sci.* **121**, 2452-2462.

Inutsuka, A., Goda, M. and Fujiyoshi, Y. (2009). Calyculin A-induced neurite retraction is critically dependent on actomyosin activation but not on polymerization state of microtubules. *Biochem. Biophys. Res. Commun.* **390**, 1160-1166.

Kasza, K. E., Nakamura, F., Hu, S., Kollmannsberger, P. B. N., Fabry, B., Stossel, T. P., Wang, N. and Weitz, D. A. (2009). Filamin A is essential for active cell stiffening but not passive stiffening under external force. *Biophys. J.* **96**, 4326-4335.

Kollmannsberger, P. and Fabry, B. (2007). High-force magnetic tweezers with force feedback for biological applications. *Rev. Sci. Instrum.* **78**, 114301.

Kollmannsberger, P. and Fabry, B. (2009). Active soft glassy rheology of adherent cells. *Soft Matter RSC* **5**, 1771-1774.

Kreidberg, J. A. (2000). Functions of alpha3beta1 integrin. *Curr. Opin. Cell Biol.* **12**, 548-553.

Leroy-Dudal, J., Demeilliers, C., Gallet, O., Pauthe, E., Dutoit, S., Agniel, R., Gauduchon, P. and Carreiras, F. (2005). Transmigration of human ovarian adenocarcinoma cells through endothelial extracellular matrix involves alphav integrins and the participation of MMP2. *Int. J. Cancer* **114**, 531-543.

Loftus, J. C. and Liddington, R. C. (1997). Cell adhesion in vascular biology. New insights into integrin-ligand interaction. *J. Clin. Invest.* **99**, 2302-2306.

Lund-Johansen, M., Bjerkvig, R., Humphrey, P. A., Bigner, S. H., Bigner, D. D. and Laerum, O. D. (1990). Effect of epidermal growth factor on glioma cell growth, migration, and invasion in vitro. *Cancer Res.* **50**, 6039-6044.

McNulty, A. L., Weinberg, J. B. and Guilak, F. (2009). Inhibition of matrix metalloproteinases enhances in vitro repair of the meniscus. *Clin. Orthop. Relat. Res.* **467**, 1557-1567.

Metzner, C., Raupach, C., Mierke, C. T. and Fabry, B. (2010). Fluctuations of cytoskeleton-bound microbeads-the effect of bead-receptor binding dynamics. *J. Phys. Condens. Matter* **22**, 194105-194113.

Mickel, W., Muenster, S., Jawerth, L. M., Vader, D. A., Weitz, D. A., Sheppard, A. P., Mecke, K., Fabry, B. and Schroeder-Turk, G. (2008). Robust pore size analysis of filamentous networks from 3D confocal microscopy. *Biophys. J.* **95**, 6072-6080.

Mierke, C. T. (2008). Role of the endothelium during tumor cell metastasis: Is the endothelium a barrier or a promoter for cell invasion and metastasis? *J. Biophys.* **2008**, 183516.

Mierke, C. T., Kollmannsberger, P., Paranhos-Zitterbart, D., Smith, J., Fabry, B. and Goldmann, W. H. (2008a). Mechano-coupling and regulation of contractility by the vinculin tail domain.. *Biophys. J.* **94**, 661-670.

Mierke, C. T., Rosel, D., Fabry, B. and Brabek, J. (2008b). Contractile forces in tumor cell migration. *Eur. J. Cell Biol.* **87**, 669-676.

Mierke, C. T., Zitterbart, D. P., Kollmannsberger, P., Raupach, C., Schlotzer-Schrehardt, U., Goecke, T. W., Behrens, J. and Fabry, B. (2008c). Breakdown of the endothelial barrier function in tumor cell transmigration. *Biophys. J.* **94** 2832-2846.

Mijailovich, S. M., Kojic, M., Zivkovic, M., Fabry, B. and Fredberg, J. J. (2002). A finite element model of cell deformation during magnetic bead twisting. *J. Appl. Physiol.* **93**, 1429-1436.

Mukhopadhyay, R., Theriault, R. L. and Price, J. E. (1999). Increased levels of alpha6 integrins are associated with the metastatic phenotype of human breast cancer cells. *Clin. Exp. Metastasis* **17**, 325-332.

Neff, N. T., Lowrey, C., Decker, C., Tovar, A., Damsky, C., Buck, C. and Horwitz, A. F. (1982). A monoclonal antibody detaches embryonic skeletal muscle from extracellular matrices. *J. Cell Biol.* **95**, 654-666.

Oakes, P. W., Patel, D. C., Morin, N. A., Zitterbart, D. P., Fabry, B., Reichner, J. S. and Tang, J. X. (2009). Neutrophil morphology and migration are affected by substrate elasticity. *Blood* **114**, 1387-1395.

Owens, D. M., Romero, M. R., Gardner, C. and Watt, F. M. (2003). Suprabasal alpha6beta4 integrin expression in epidermis results in enhanced tumourigenesis and disruption of TGFbeta signalling. *J. Cell Sci.* **116**, 3783-3791.

Palecek, S. P., Loftus, J. C., Ginsberg, M. H., Lauffenburger, D. A. and Horwitz, A. F. (1997). Integrin-ligand binding properties govern cell migration speed through cell-substratum adhesiveness. *Nature* **385**, 537-540.

Paszek, M. J., Zahir, N., Johnson, K. R., Lakins, J. N., Rozenberg, G. I., Gefen, A., Reinhart-King, C. A., Margulies, S. S., Dembo, M., Boettiger, D. et al. (2005). Tensional homeostasis and the malignant phenotype. *Cancer Cell* **8**, 241-254.

Pelham, R. J., Jr and Wang, Y. (1997). Cell locomotion and focal adhesions are regulated by substrate flexibility. *Proc. Natl. Acad. Sci. USA* **94**, 13661-13665.

Potdar, A. A., Jeon, J., Weaver, A. M., Quaranta, V. and Cummings, P. T. (2010). Human mammary epithelial cells exhibit a bimodal correlated random walk pattern. *PLoS ONE* **5**, e9636.

Qian, F., Zhang, Z. C., Wu, X. F., Li, Y. P. and Xu, Q. (2005). Interaction between integrin alpha(5) and fibronectin is required for metastasis of B16F10 melanoma cells. *Biochem. Biophys. Res. Commun.* **333**, 1269-1275.

Raupach, C., Zitterbart, D. P., Mierke, C. T., Metzner, C., Muller, F. A. and Fabry, B. (2007). Stress fluctuations and motion of cytoskeletal-bound markers. *Phys. Rev. E Stat. Nonlin. Soft Matter Phys.* **76**, 011918.

Rösel, D., Brabek, J., Tolde, O., Mierke, C. T., Zitterbart, D. P., Raupach, C., Bicanova, K., Kollmannsberger, P., Pankova, D., Vesely, P. et al. (2008). Up-regulation of Rho/ROCK signaling in sarcoma cells drives invasion and increased generation of protrusive forces. *Mol. Cancer Res.* **6**, 1410-1420.

Sawada, K., Mitra, A. K., Radjabi, A. R., Bhaskar, V., Kistner, E. O., Tretiakova, M., Jagadeeswaran, S., Montag, A., Becker, A., Kenny, H. A. et al. (2008). Loss of E-cadherin promotes ovarian cancer metastasis via alpha 5-integrin, which is a therapeutic target. *Cancer Res.* **68**, 2329-2339.

Schirner, M., Herzberg, F., Schmidt, R., Streit, M., Schoning, M., Hummel, M., Kaufmann, C., Thiel, E. and Kreuser, E. D. (1998). Integrin alpha5beta1: a potent inhibitor of experimental lung metastasis. *Clin. Exp. Metastasis* **16**, 427-435.

Steeg, P. S. (2006). Tumor metastasis: mechanistic insights and clinical challenges. *Nat. Med.* **12**, 895-904.

Tani, N., Higashiyama, S., Kawaguchi, N., Madarame, J., Ota, I., Ito, Y., Ohoka, Y., Shiosaka, S., Takada, Y. and Matsuura, N. (2003). Expression level of integrin alpha 5 on tumour cells affects the rate of metastasis to the kidney. *Br. J. Cancer* **88**, 327-333.

Taverna, D., Ullman-Cullere, M., Rayburn, H., Bronson, R. T. and Hynes, R. O. (1998). A test of the role of alpha5 integrin/fibronectin interactions in tumorigenesis. *Cancer Res.* **58**, 848-853.

Vleminckx, K., Vakaet, L., Jr, Mareel, M., Fiers, W. and van Roy, F. (1991). Genetic manipulation of E-cadherin expression by epithelial tumor cells reveals an invasion suppressor role. *Cell* **66**, 107-119.

Voura, E. B., Ramjeesingh, R. A., Montgomery, A. M. and Siu, C. H. (2001). Involvement of integrin alpha(v)beta(3) and cell adhesion molecule L1 in transendothelial migration of melanoma cells. *Mol. Biol. Cell* **12**, 2699-2710.

Wang, N., Naruse, K., Stamenovic, D., Fredberg, J. J., Mijailovich, S. M., Tolic-Norrelykke, I. M., Polte, T., Mannix, R. and Ingber, D. E. (2001). Mechanical behavior in living cells consistent with the tensegrity model. *Proc. Natl. Acad. Sci. USA* **98**, 7765-7770.

Webb, D. J., Donais, K., Whitmore, L. A., Thomas, S. M., Turner, C. E., Parsons, J. T. and Horwitz, A. F. (2004). FAK-Src signalling through paxillin, ERK and MLCK regulates adhesion disassembly. *Nat. Cell Biol.* **6**, 154-161.

Wolf, K., Mazo, I., Leung, H., Engelke, K., von Andrian, U. H., Deryugina, E. I., Strongin, A. Y., Brocker, E. B. and Friedl, P. (2003). Compensation mechanism in tumor cell migration: mesenchymal-amoeboid transition after blocking of pericellular proteolysis. *J. Cell Biol.* **160**, 267-277.

Wu, H., Liang, Y. L., Li, Z., Jin, J., Zhang, W., Duan, L. and Zha, X. (2006). Positive expression of E-cadherin suppresses cell adhesion to fibronectin via reduction of alpha5beta1 integrin in human breast carcinoma cells. *J. Cancer Res. Clin. Oncol.* **132**, 795-803.

Zaman, M. H., Trapani, L. M., Siemeski, A., Mackellar, D., Gong, H., Kamm, R. D., Wells, A., Lauffenburger, D. A. and Matsudaira, P. (2006). Migration of tumor cells in 3D matrices is governed by matrix stiffness along with cell-matrix adhesion and proteolysis. *Proc. Natl. Acad. Sci. USA* **103**, 10889-10894.

Journal of Cell Science